UNIVERSITY OF CALIFORNIA
RIVERSIDE

Tackling Optimization Challenges in Industrial Load Control and Full-Duplex Radios

A Dissertation submitted in partial satisfaction
of the requirements for the degree of

Doctor of Philosophy

in

Electrical Engineering

by

Armen Gholian

June 2015

Dissertation Committee:
- Dr. Yingbo Hua, Co-Chairperson
- Dr. Hamed Mohsenian-Rad, Co-Chairperson
- Dr. Ertem Tuncel

The Dissertation of Armen Gholian is approved:

_____

_____

Committee Co-Chairperson

_____

Committee Co-Chairperson

University of California, Riverside

Acknowledgments

First of all, I want to thank my advisor, Dr. Yingbo Hua, for his valuable guidance and full support throughout my PhD studies. His office door has always been open to me and he has always addressed any concern patiently and thoughtfully.

I also want to thank my co-advisor, Dr. Hamed Mohsenian-Rad, for his great research guidance. He has always been to the point and quick in addressing any issue. It has been very inspiring working with him.

I also want to thank my friends at UCR. Particularly, my friends in Laboratory of Signals, Systems and Networks, Shenyang Xu, Ali Cagatay Cirik, Qian Gao, Yiming Ma, and Yifan Li. And my friends in Laboratory of Smart Grid, Hossein Akhavan-Hejazi, Mahdi Ghamkhari, Sajjad Amini, and Mahdi Kohansal.

Finally, I want to thank my mom, Volga, whom I owe everything. And my sisters, Melina and Midia, and my brother, Arin, for their unconditional love and support.

To my family.

ABSTRACT OF THE DISSERTATION

Tackling Optimization Challenges in Industrial Load Control and Full-Duplex Radios

by

Armen Gholian

Doctor of Philosophy, Graduate Program in Electrical Engineering
University of California, Riverside, June 2015
Professor Yingbo Hua, Co-Chairperson
Professor Hamed Mohsenian-Rad, Co-Chairperson

In price-based demand response programs in smart grid, utilities set the price in accordance with the grid operating conditions and consumers respond to price signals by conducting optimal load control to minimize their energy expenditure while satisfying their energy needs. Industrial sector consumes a large portion of world electricity and addressing optimal load control of energy-intensive industrial complexes, such as steel industry and oil-refinery, is of practical importance. Formulating a general industrial complex and addressing issues in optimal industrial load control in smart grid is the focus of the second part of this dissertation. Several industrial load details are considered in the proposed formulation, including those that do not appear in residential or commercial load control problems. Operation under different smart pricing scenarios, namely, day-ahead pricing, time-of-use pricing, peak pricing, inclining block rates, and critical peak pricing are considered. The use of behind-the-meter renewable generation and energy storage is also considered. The formulated optimization problem is originally nonlinear and nonconvex and thus hard to

solve. However, it is then reformulated into a tractable linear mixed-integer program. The performance of the design is assessed through various simulations for an oil refinery and a steel mini-mill.

In the third part of this dissertation, a novel all-analog RF interference canceler is proposed. Radio self-interference cancellation (SIC) is the fundamental enabler for full-duplex radios. While SIC methods based on baseband digital signal processing and/or beamforming are inadequate, an all-analog method is useful to drastically reduce the self-interference as the first stage of SIC. It is shown that a uniform architecture with uniformly distributed RF attenuators has a performance highly dependent on the carrier frequency. It is also shown that a new architecture with the attenuators distributed in a clustered fashion has important advantages over the uniform architecture. These advantages are shown numerically through random multipath interference channels, number of control bits in step attenuators, attenuation-dependent phases, single and multi-level structures, etc.

Contents

List of Figures

List of Tables

Part I

Introduction

Chapter 1

Introduction

This dissertation addresses two types of challenging optimization problems in two application areas: industrial load control in smart grid and full-duplex radios in communications.

The second part of the dissertation is on optimal industrial load control in smart grid. Smart grid is the future electric power system where consumers may *participate* in the operation of the grid through demand response, distributed generation, and distributed energy storage. The main driver for consumers to participate such programs is to reduce their electricity cost. From the utility company's perspective, customer participation can be used to balance supply and demand and consequently, to reduce the overall power generation and power system operation cost.

Demand response programs mostly are usually in two forms: direct load control (DLC) and *smart pricing*. In DLC programs, based on an agreement between the utility company and consumers, the utility company controls the operations and energy consump-

tion of certain units of consumers. DLC programs are not very popular among consumers mainly due to privacy concerns and lack of control of users over their units. On the other hand, in smart pricing, consumers are encouraged to respond to the price signals through *optimal load control* by shifting or changing consumption of any *controllable load* to minimize their electricity cost while satisfying their energy needs.

Since over 40% of world electricity consumption is by industrial sector, addressing optimal industrial load control is of importance. Interestingly, optimal load control for industrial users is more convenient than for residential and commercial users since (1) many industries are already automated and one can benefit from these existing automation infrastructure and upgrade them with control mechanisms that take into consideration power usage and demand response, and (2) in contrast to residential users where user might sacrifice electricity cost in order to have higher comfort level, for industrial users comfort level is not of importance and the only design objective is profit. However, optimal industrial load control is a challenging task and requires addressing issues that do not appear in residential or commercial load control. For example, a key aspect in industrial load control is the *inter-process dependency* in industrial processes, where the operation of a processes depends on the material that is provided by one or more other processes.

Addressing these and other challenges in industrial load control is the focus in the second part of the dissertation. Particularly, industrial load control optimization problem under two cases, basic and comprehensive, are formulated. In the basic case, each industrial unit is processing a constant amount of material at each cycle and its electricity load is constant at each cycle. In the comprehensive case, an industrial unit may take different

amount of material at each cycle and its electricity load has an affine relationship with the amount of material processed.

In addition, important industrial load constraints such as inter-dependency among industrial units, uninterruptiblity of the industrial units, maximum load constraint, material balance, material proportionality, and material storage are considered in the formulation. Operation under different smart pricing scenarios including day-ahead pricing, time-of-use pricing, peak pricing, inclining block rates, and critical peak pricing is considered. The use of behind-the-meter renewable generation and energy storage are also taken into consideration.

The formulated industrial load control optimization problem is a tractable mixed-integer linear program. Case studies of oil refinery and steel mini-mill are also presented. Most of the contents of this part are published in [1, 2].

The third part of the dissertation is on *full-duplex* radios. Full-duplex devices are devices that can transmit and receive at the same time and in the same frequency band. The main challenge in full-duplex is that the transmitted signal created by the device's own transmitter, known as *self-interference*, is very strong at its own receiver. By canceling self-interference to the noise floor, full-duplex would be realizable and the throughput would be doubled. There are different methods for self-interference cancellation (SIC).

Two major methods for SIC are *all-analog* and *all-digital*. An all-analog method cancels RF interference at RF frontend by using its RF interference source. An all-digital method cancels interference only after the interference has been converted into baseband and digitized.

Here, we propose a novel architecture for all-analog cancellation called *clustered*

architecture and compare its performance with uniform architecture. Through simulation, it is shown that in addition that the performance of the clustered canceler is as good or better than the uniform canceler, its performance is also independent of the carrier frequency. We also evaluate statistical limits of the proposed architecture of both clustered and uniform cancelers for ideal and non-ideal attenuators. Furthermore, we consider a wide range of realizations of a random interference channel model. We show how the cancellation performance in each architecture varies as the number of taps, relative delay between two adjacent taps, path loss, bandwidth, the number of control bits and phase of the attenuators change. We also investigate impact of randomized uniform and multi-level cancellation. Most of the contents of this part are published in [3, 4].

Chapter 2

Mathematical Background

An optimization problem has the following general format:

$$\begin{aligned} \underset{x}{\text{minimize}} \quad & f_0(x) \\ \text{subject to} \quad & f_i(x) \leq 0,\ i = 1, \ldots, m \\ & h_i(x) = 0,\ i = 1, \ldots, p \end{aligned} \tag{2.1}$$

Here, elements of the vector $x \in R^n$ are the *decision variables*, function $f_0 : R^n \to R$ is the *objective function*, and $f_i(x) \leq 0$ and $h_i(x) = 0$ are the inequality and equality *constraints*, respectively. The goal is find an x that minimizes $f_0(x)$ among all choices of vector x that satisfy the constraints.

Any point that satisfies the constraints is a *feasible point*. The set of all feasible points is called the *feasible set*. An optimization problem is said to be *infeasible* if the feasible set is the empty set.

Three important categories of optimization are considered here: linear optimiza-

tion, convex optimization, and mixed-integer programming.

Optimization problems can be classified in different ways. One classification is if the optimization problem is convex or not. The advantage of having a convex optimization problem is that it can be solved reliably and efficiently. Note that linear optimization is a special case of convex optimization. Another classification of optimization problems is based on if there is a discrete decision variable in the problem or not. Optimization problems with discrete decision variables are generally difficult to solve. Note that there is no discrete decision variable in linear and convex optimization problems.

2.1 Linear Optimization

Function $f : R^n \to R^m$ is an *affine function* if it is a sum of a linear function and a constant, i.e., if it has the form $f(x) = Ax + b$, where $A \in R^{m\times n}$ and $b \in R^m$.

Optimization problem (2.5) is a *linear optimization* problem if $f_i(x)$ and $h_i(x)$ are affine functions. Hence, a linear optimization problem has the following form:

$$\begin{aligned} \underset{x}{\text{minimize}} \quad & c^T x + d \\ \text{subject to} \quad & A_{ineq}x + b_{ineq} \leq 0 \\ & A_{eq}x + b_{eq} = 0 \end{aligned} \tag{2.2}$$

where $c \in R^n, d \in R, A_{ineq} \in R^{m\times n}, b_{ineq} \in R^m, A_{eq} \in R^{p\times n}$, and $b_{eq} \in R^p$.

There are a variety of very effective methods for solving linear optimization problems reliably and efficiently, including simplex method [5, 6] and interior-point methods [7]. There are many solvers for linear optimization problems, including MATLAB function *linprog* and CVX [8]. Linear optimization is also known as linear programming (LP).

2.2 Convex Optimization

Before defining a convex optimization, convex sets and convex functions should be defined. C is a *convex set* if for any $x_1, x_2 \in C$ and any θ with $0 \leq \theta \leq 1$, we have [7]

$$\theta x_1 + (1 - \theta)x_2 \in C. \tag{2.3}$$

f is a *convex function* if domain of f is a convex set and if for all x, y in domain of f, and θ with $0 \leq \theta \leq 1$, we have [7]

$$f(\theta x + (1 - \theta)y) \leq \theta f(x) + (1 - \theta)f(y) \tag{2.4}$$

An optimization problem is a *convex optimization* if it has the following form:

$$\begin{aligned} \underset{x}{\text{minimize}} \quad & f_0(x) \\ \text{subject to} \quad & f_i(x) \leq 0,\ i = 1, \ldots, m \\ & a_i^T x + b_i = 0,\ i = 1, \ldots, p \end{aligned} \tag{2.5}$$

where f_0 and $f_1, \ldots, f_m$ are convex functions. Hence, in a convex optimization, a convex objective function is minimized over a convex set. Clearly, linear optimization problems are a subset of convex optimization problems.

Similar to linear programming, there are very effective algorithms to solve convex optimization problems reliably and efficiently, such as interior-point methods [7]. There are also several solvers for convex optimization problems including CVX [8].

2.3 Mixed-Integer Programming

In linear and convex optimization problems, decision variables are continuous. However, a decision variable may be discrete as well. In practice, discrete variables are often

integer. An optimization problem is an *integer program* if the decision variables take only integer values within a certain range. An optimization problem is a *mixed-integer program* (MIP) if some decision variables are integer and some are continuous. An optimization problem is a *mixed-integer linear programming* (MILP) if it is a linear optimization problem with a mix of integer and continuous decision variables.

Integer programs and mixed-integer programs are generally difficult to solve. However, there are effective methods to solve MILPs, such as branch and bound method [9]. In practice, MILPs are solved using various optimization software including CPLEX [10] and MOSEK [11].

Major optimization software such as CPLEX uses *branch-and-cut* method to solve MIP and MILP problems. The branch-and-cut method searches a tree consisting of *nodes*. Every node represents a linear programming (LP) or quadratic programming (QP) subproblem to be processed, i.e., to be solved and to be checked for integrality. Nodes that are not processed yet are called *active* nodes. The search in tree continues until either no more active node is available or a stopping condition is met.

A *branch* is the creation of two new nodes from a parent node. A branch occurs when the bounds on a single variable are changed, with the new bounds remaining in effect for that new node and for any of its descendants. For instance, if a branch occurs on a binary variable with a lower bound of 0 and an upper bound of 1, then the result will be two new nodes, one node with a modified upper bound of 0, and the other node with a modified lower bound of 1. As a result, the two new nodes will have completely distinct feasible sets.

A *cut* is a constraint that is added to the model. The purpose of a cut is to reduce the size of the feasible set for the continuous LP or QP problems represented at the nodes, while not eliminating possible integer solutions. Consequently, a cut would reduce the number of branches required to solve the MILP of interest.

The branch-and-cut method, then, consists of performing branches and applying cuts at the nodes of the tree. A more detailed outline of the steps is as follows [10]. First, the branch-and-cut tree is initialized to have the root node as the only active node where the root node is the entire problem, ignoring all of the explicit integrality requirements. Then, potential cuts are generated for the root node. Also, if possible, an *incumbent solution* (that is, the best known solution that satisfies all the integrality requirements) is established at this point for later use in the procedure.

When processing a node, first the continuous relaxation of its subproblem is solved, i.e., the subproblem without integrality constraints. Then, it is checked to see if the obtained solution satisfies the integrality constraints. If so, and if its objective value is better than the current incumbent, the obtained solution is used as the new incumbent. If not, branching will occur. The branch is applied on a variable where the value of the present solution violates its integrality requirement. This results in two new nodes being added to the tree.

Each node, after its relaxation is solved, possesses an optimal objective function value Z. At any given point in the algorithm, there is a node whose Z value is better (less, in the case of a minimization problem, or greater for a maximization problem) than all the others. This *best node* value can be compared to the objective function value of the incumbent solution. The resulting MIP Gap, expressed as a percentage of the incumbent

solution, serves as a measure of progress toward finding and proving optimality. When active nodes no longer exist, then these two values will have converged toward each other, and the MIP Gap will be zero, signifying that optimality of the incumbent has been proven.

In practice, most MIP and MILP software allow terminating the branch-and-cut procedure before proving the optimality of the incumbent. For example, in CPLEX [10], a user can set a time limit or a limit on the number of nodes to be processed. With default settings, it will terminate the search when the MIP Gap has been brought lower than 0.0001 (0.01%).

Part II

Optimal Industrial Load Control in Smart Grid

Chapter 3

Introduction and Related Work

To assure reliable service, electricity generation capacity is often designed to match the *peak demand*. Accordingly, it is desirable to minimize the peak-to-average ratio (PAR) in the aggregated demand profile in order to achieve efficient operation and minimize the need to build new power plants. This can be done by a combination of *smart pricing* by utility companies and *optimal load control* by consumers. While the former has been widely studied in the demand response (DR) literature, e.g. [12–17], the latter is also of critical importance, where the focus is on exploiting the *controllable load* potential in each load sector in response to changes in price signals.

Most prior work on optimal load control are concerned with residential [18–21] and commercial [22, 23] loads. However, since the industrial sector comprises 42% of the world's electricity consumption [1], addressing industrial load control (ILC) is also critical. Interestingly, since many industries are already automated, one can benefit from these existing automation infrastructure and upgrade them with control mechanisms that take

into consideration power usage and demand response. Table 3.1 shows some factors that make industrial load control different from residential load control.

Table 3.1: Industrial vs. residential load control

Design Factor	**Residential**	**Industrial**
Peak Load Shaving	✓	✓
Time-Shiftable Load	✓	✓
Interruptible Load	✓	✓
Uninterruptible Load	✓	✓
Pricing Tariffs	✓	✓
On-site Renewable Generation	✓	✓
On-site Energy Storage	✓	✓
Sequential Operation		✓
Load Dependency		✓
Size of Batch Cycles		✓
Number of Batch Cycles		✓
Material Flow		✓
Material Balance		✓
Material Storage		✓
Final Products		✓
By-products		✓
Human Comfort	✓	

Note that due to the existence of discrete decision variables in formulation of industrial load control, e.g., unit on/off, optimal industrial load control problems are inherently (mixed) integer programming problems [24].

This study can be compared, e.g., with [1, 25–29]. In [25], the benefits and challenges in ILC-based demand response are discussed; however, no specific design formulation is presented. In [26], an ILC algorithm is proposed; however, some important industrial load features, such as the operational interdependency across industrial units are not formulated. Such details are partly discussed in [27–29]; however, neither [26] nor [27–29] considers size and the number of batch cycles in their formulations and whether each industrial unit is

interruptible or uninterruptible. Furthermore, the analyses in these studies do not include the emerging smart grid components, such as different smart pricing tariffs and the use of local renewable generation and energy storage. Finally, compared to our earlier work in [1], this paper has three advantages. First, here we manage both energy usage and material flow. Second, here, we incorporate a wider range of smart pricing models and also address local renewable generators and energy storage. Third, the system model in [1] is inherently limited to a single batch cycle. In contrast, here we model several batch processing cycles and accordingly conduct optimal ILC over multi-day operation horizons.

Here, an *industry* is defined as a collection of several industrial units or processes. A process is either *batch* or *continuous*. In a batch process, the input materials are fed into a unit at the beginning of each batch processing cycle. The processed material are collected at the end of the batch processing cycle. In contrast, in a continuous process, materials are fed and/or products are produced continuously [24, 30]. While most batch processes have controllable load potential, continuous processes are often uncontrollable loads. Accordingly, here, the power usage for continuous processes is considered as uncontrollable background load while power usage for batch processes is considered as potential *controllable load*.

Industrial load control is explained in two chapters. In chapter 4, an industrial load control model for industries in which an industrial unit is processing a constant amount of material at each cycle and its electricity load is constant at each cycle, is presented. In chapter 5, a more comprehensive industrial load control model in which an industrial unit may take different amount of material at each cycle and its electricity load has an affine relationship with the amount of material processed, is presented.

Nomenclature

$\mathcal{T}$, t	Set and index of time slots.
T	Scheduling horizon.
$\mathcal{V}$, i	Set and index of industrial units.
$\mathcal{K}$, k	Set and index of materials.
$\mathcal{R}$, r	Set and index of initial/raw materials, $\mathcal{R} \subset \mathcal{K}$.
$\mathcal{F}$, f	Set and index of final materials/products, $\mathcal{F} \subset \mathcal{K}$.
a_i	Number of time slots in unit i's each batch cycle.
$s_i[t]$	Number of unit i's batch cycles started up to time t.
$e_i[t]$	Number of unit i's batch cycles finished up to time t.
$x_i[t]$	Indicating whether unit i operates at time slot t.
$u_i[t]$	Total material that is fed to unit i at time t.
$y_i[t]$	Total material that is produced by unit i at time t.

α_i Minimum material capacity of unit i.

β_i Maximum material capacity of unit i.

$m_k[t]$ Amount of material k available at storage at time t.

η_k Capacity of storage for material k.

ϕ_f Minimum amount of final product f that is needed.

$m_k[0]$ Initial amount of material k available in storage.

$M_i[t]$ Total amount of all materials inside unit i at time t.

$\mathcal{I}_k^{in}$ Set of units that use material k as an input.

$\mathcal{I}_k^{out}$ Set of units that produce material k as an output.

r_i^k Required fraction of material k at the input of unit i.

q_i^k Fraction of material k at the output of unit i.

$\mathcal{I}_{unt}$ Set of uninterruptible units.

$\mathcal{K}_{imd}$ Set of non-storable materials.

l_i Electricity consumption of unit i per time slot.

$l_i[t]$ Electricity consumption of unit i at time slot t.

c_i, d_i Parameters of electricity consumption of unit i.

l_i^{min} Minimum stand-by electricity consumption of unit i.

$l_{back}[t]$ Background load at time slot t.

$L[t]$ Total electricity consumption of complex at time t.

L_{max} Power draw limit of the industrial complex.

$p[t]$ Price of electricity at time slot t.

p_f Unit price of final product f.

p_r Unit price of initial/raw material r.

γ_k Cost of storing a unit of material k for one time slot.

C_{elct} Electricity cost during scheduling horizon.

C_{fixed} Fixed cost of the industrial complex.

$b[t]$ Indicating status of the battery system at time t.

$l_{ch}[t]$ Charge amount of the battery system at time t.

$l_{dch}[t]$ Discharge amount of the battery system at time t.

l_{ch}^{max} Maximum charge rate of the battery system.

l_{dch}^{max} Maximum discharge rate of the battery system.

μ Efficiency of the battery system during charge.

θ Efficiency of the battery system during discharge.

B^{init} Initial charge levels of the battery system.

B^{full} Capacity of the battery system.

$l_{slr}[t]$ Expected value of available solar energy at time t.

Ω A large enough number.

Chapter 4

Basic Industrial Load Control: A Case Study for Oil Refineries

In this chapter a model for optimal industrial load control is proposed in which each industrial unit is processing a constant amount of material at each cycle and its electricity load is constant at each cycle. Most contents of this chapter is also published in [1].

The contributions in this chapter are summarized as follows:

- We take several industrial load details into consideration, including those that do not appear in residential or commercial load control problems. For example, operation completion constraints, sequential operation constraints, immediate start constraints, uninterruptable operation constraints, and maximum load constraints.
- The formulated industrial load control optimization problem is a tractable binary linear program.

- A case study of oil renery is included.

4.1 Oil Refinery Industry

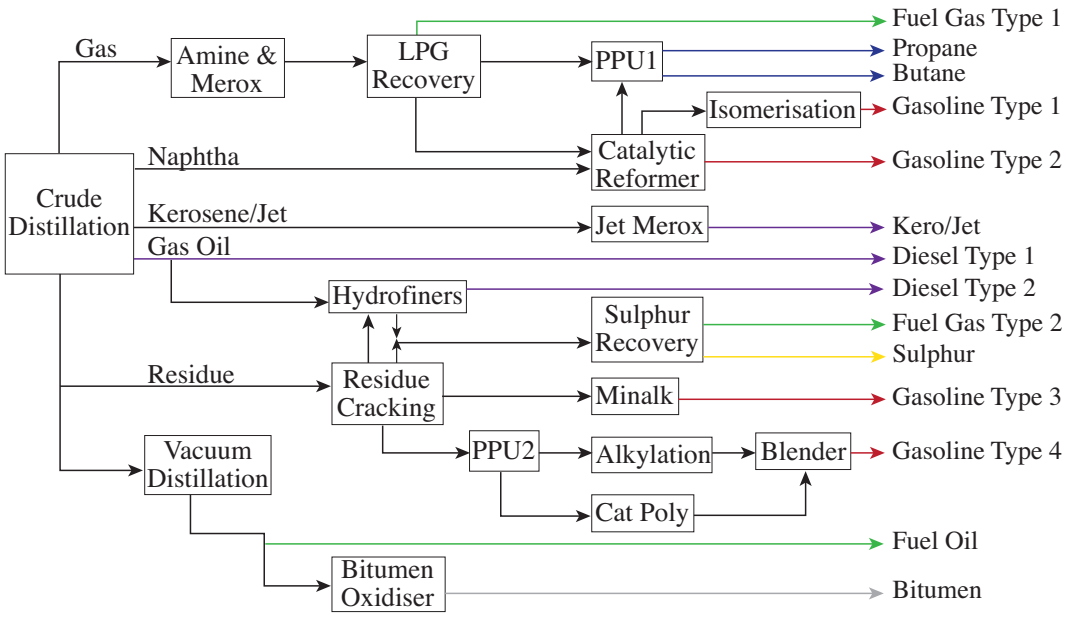

Figure 4.1: Flow diagram of crude oil processing at the BP Kwinana Oil Refinery with 17 processing units and 14 different final products [31].

4.1.1 Background

In this section, we provide a brief overview of a typical crude oil processing facility, based on the example of the BP Kwinana refinery [31]. The flow diagram of the processes is shown in Fig. 4.1. Crude oil, which is a combination of various hydrocarbons, is first distilled in the Crude Distillation Unit, where it is divided into a number of fractions including gas, naphtha, kerosene, gas oil, and residue. The Amine and Merox unit then removes hydrogen sulfide and/or mercaptans from gas. In the LPG Recovery Unit, liquid petroleum gas (LPG)

is recovered. The Catalytic Reformer further processes the naphtha and gasoline that come from the Crude Distillation Unit to make them suitable components for blending into motor spirit. LPG is fed to the Propane Production Unit 1 (PPU1) for separation into propane and butane. The Isomerisation Unit uses a process designed to upgrade the octane number of Light Hydrotreated Naphtha from the Catalytic Reformer. The Jet Merox Unit takes Jet from the Crude Distillation Unit and removes the mercaptans. The Residue Cracking Unit breaks down the long chain hydrocarbons into smaller, more valuable components. The Hydrofiners enable the refinery to process sour crude, which has higher sulphur content. Hydrofiner takes Light Cycle Oil from the Residue Cracking Unit and both take gas oil from the Crude Distillation Unit. Sulphur is removed through a hydrotreating process, and the result is the sweetened oil that is blended to make diesel. The Sulphur Recovery Unit removes sulphur from gas streams that could otherwise contribute to atmospheric emissions. The PPU2 takes LPG from the Residue Cracking Unit and removes hydrogen sulphide and mercaptan sulphur. The mixed LPG is then split into C3 and C4 streams. The C3 stream can be sold directly or be passed to the Catalytic Polymerisation Unit (CPU) for further processing. The bulk of the C4 stream goes to the Alkylation Unit, while the remainder goes to the CPU. The Alkylation unit combines smaller molecules to produce high-octane motor spirit. Vacuum Distillation Unit distills the residue further. Finally, Bitumen is made from the heavy ends of crude oil by the Vacuum Distillation Unit [31].

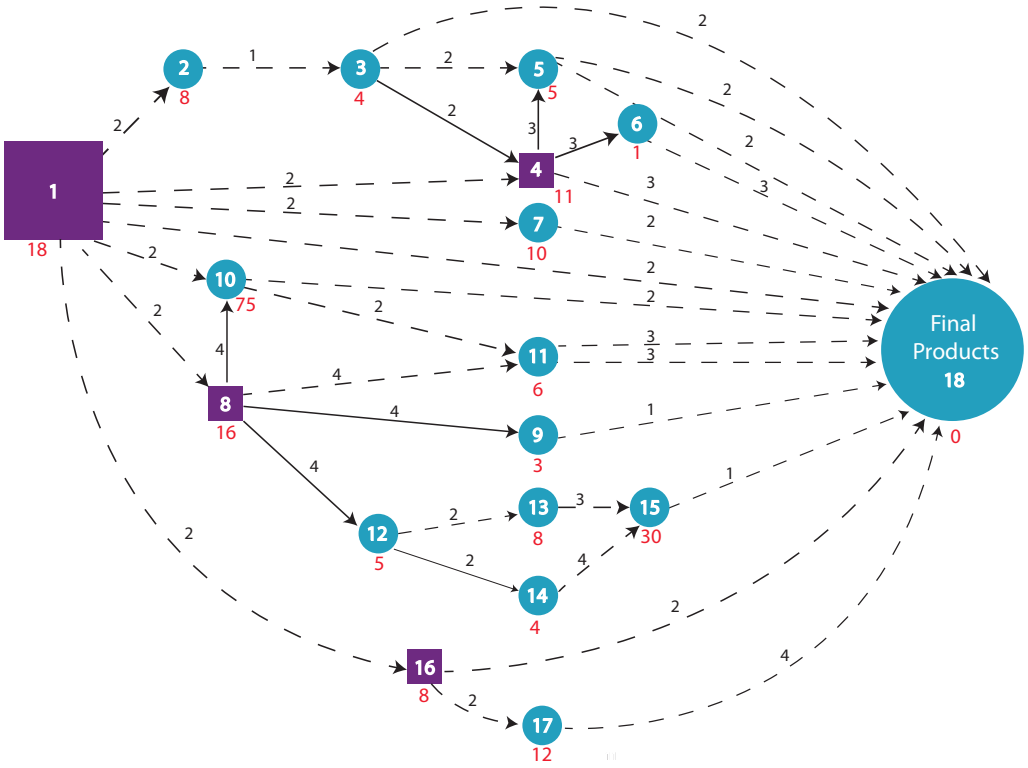

Figure 4.2: Directed graph representation of the flow diagram in Fig. 4.1.

4.1.2 Directed Graph Representation

In this section, we provide a *directed acyclic graph representation* of the inter-connecting units inside an industrial complex. Our focus is again on the example of an oil refinery. The directed graph representation of the inter-connecting units in the BP Kwinana Refinery is shown in Fig. 4.2. In total, there are 18 nodes in this graph. Nodes 1 to 17 represent the processing units in the following order: Crude Distillation, Amine & Merox, LPG Recovery, Catalytic Reformer, PPU1, Isomerisation, Jet Merox, Residue Cracker, Minalk, Hydrofiners, Sulphur Recovery, PPU2, Alkylation, Cat Poly, Blender, Vacuum Distillation, and Bitumen Oxidiser. The last (i.e., the 18th) node is labeled as Final Products and represents the unit that collects and exports the final products.

The graph edges indicate the presence and type of inter-dependencies among the units. In particular, the directed edge (i, j) from node i to node j indicates that node i is a feeding unit of node j; therefore, node j may start operation only if the operation of node i is finished. For each edge (i, j), the weight $a_{i,j}$ indicates the time (in terms of 15 minutes time slots) that it will take for unit i to finish its operation[1] . As an example, consider edge $(4, 6)$ with weight $a_{4,6} = 3$. This indicates that unit 6 may not start operation until unit 4 finishes its operation. It also indicates that it will take 3 time slots, i.e., $3 \times 15 = 45$ minutes for unit 4 for finish its operation. Also note that some nodes may have multiple incoming edges. For example, node 15 has an incoming edge from node 13 and another incoming edge from node 14. This is because both units 13 and 14 are feeding units for unit 15.

[1]The edge weights include hold-up times, i.e., the time required to transport the processed materials from one unit to the next. It is assumed that electricity consumption of a unit remains the same during the hold-up time.

The directed graph representation in Fig. 4.2 can explain the sequence of processes that lead to each final product. For example, to produce Fuel Gas Type 1, the following operational sequence can be identified. First, unit 1 should operate for $2 \times 15 = 30$ minutes. Then, unit 2 should operate for $1 \times 15 = 15$ minutes. After that, unit 3 should operate for $2 \times 15 = 30$ minutes. Hence, from the moment that unit 1 starts its operation, it will take at least $(2 + 1 + 2) \times 15 = 75$ minutes before Fuel Gas Type 1 can be ready. Similar operational sequences can be identified for other final products.

Each edge can be either a solid line or dashed line, based on the type of dependencies among units. Solid edges indicate the requirement for immediate start, while dashed edges indicate the flexibility for a delayed start. For example, consider the solid edge $(8, 9)$. It indicates that the operation of unit 9 must start immediately after the operation of unit 8 is complete. In contrast, the dashed edge $(2, 3)$ indicates that the operation of unit 3 can be started any time (i.e., with delay, if needed) after the operation of unit 2 is complete.

Each node can be represented by either a circle or a square. Circle nodes are interruptable units. For example, consider unit 12, which has outgoing edges with weight 2. The operation of this unit is complete after $2 \times 15 = 30$ minutes, whether it is a consecutive 30 minutes or two separate 15 minutes. In contrast, square nodes are uninterruptable units which are less flexible. For example, consider unit 8, which has outgoing edges with weight 4. The operation of this unit is complete after $4 \times 15 = 60$ minutes. However, since unit 8 is uninterruptable, it may only operate in a consecutive 60 minutes. That is, it cannot operate at four separate 15 minutes or two separate 30 minutes. Once an uninterruptable unit starts operation it cannot be switched off until it finishes its operation.

Finally, there is a per-time slot electricity consumption associated with each unit. For example, the per-time slot electricity consumption associated with unit 8 is 16 kWh. Since the operation of unit 8 is completed in 4 times lots, the total electricity consumption of unit 8 to finish operation is $4 \times 16 = 64$ kWh. Of course, since unit 8 is an uninterruptable unit, it must consume 64 kWh in a single one-hour period.

Note that in [31], BP did not release enough information to allow us set the numbers for weights of edges, weights of nodes, types of edges, and types of nodes according to BP's actual facility. However, for the purpose of demonstration, some data shown in Fig. 4.2 are collected and scaled from other sources including [32], and the rest are chosen randomly.

4.1.3 Potential for Load Control

To gain insight about the potential for designing an industrial load control for the processes in the oil refinery described in Figs. 4.1 and 4.2, consider the two energy consumption scheduling examples in Fig. 4.3. Both schedules are acceptable in the sense that they both satisfy the operational requirements that we described in Section 4.1.2. However, if the price of electricity is not flat, then the electricity cost of implementing these two energy consumption schedules can be very different. In fact, for the sample day-ahead electricity prices shown in the second to last row in Figs. 4.3(a) and 4.3(b), the electricity cost of the first schedule becomes \$26.5, while the electricity cost of the second schedule becomes \$16.1, i.e., 40% less. These simple examples show that there is a great potential to reduce the energy expenditure of this case study if appropriate load control is implemented.

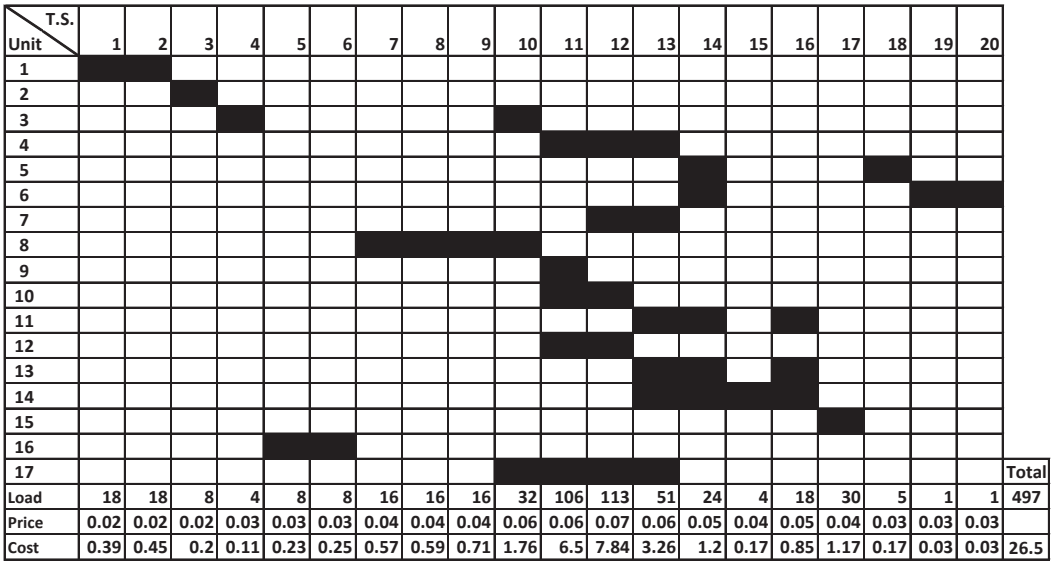

T.S. / Unit	1	2	3	4	5	6	7	8	9	10	11	12	13	14	15	16	17	18	19	20	
1																					
2																					
3																					
4																					
5																					
6																					
7																					
8																					
9																					
10																					
11																					
12																					
13																					
14																					
15																					
16																					
17																					Total
Load	18	18	8	4	8	8	16	16	16	32	106	113	51	24	4	18	30	5	1	1	497
Price	0.02	0.02	0.02	0.03	0.03	0.03	0.04	0.04	0.04	0.06	0.06	0.07	0.06	0.05	0.04	0.05	0.04	0.03	0.03	0.03	
Cost	0.39	0.45	0.2	0.11	0.23	0.25	0.57	0.59	0.71	1.76	6.5	7.84	3.26	1.2	0.17	0.85	1.17	0.17	0.03	0.03	26.5

(a)

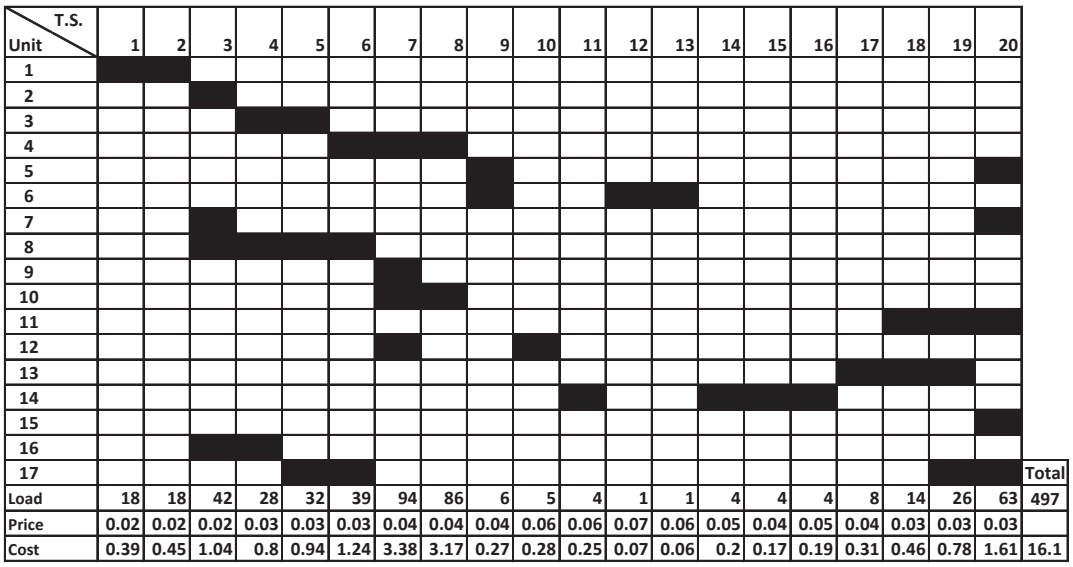

T.S. / Unit	1	2	3	4	5	6	7	8	9	10	11	12	13	14	15	16	17	18	19	20	
1																					
2																					
3																					
4																					
5																					
6																					
7																					
8																					
9																					
10																					
11																					
12																					
13																					
14																					
15																					
16																					
17																					Total
Load	18	18	42	28	32	39	94	86	6	5	4	1	1	4	4	4	8	14	26	63	497
Price	0.02	0.02	0.02	0.03	0.03	0.03	0.04	0.04	0.04	0.06	0.06	0.07	0.06	0.05	0.04	0.05	0.04	0.03	0.03	0.03	
Cost	0.39	0.45	1.04	0.8	0.94	1.24	3.38	3.17	0.27	0.28	0.25	0.07	0.06	0.2	0.17	0.19	0.31	0.46	0.78	1.61	16.1

(b)

Figure 4.3: Two example energy consumption schedules to implement the flow diagram of Fig. 4.1. While both schedules are acceptable, the electricity cost of implementing the schedule in (b) is significantly less than that of in (a).

4.2 Optimal Industry Load Control

In this section, we formulate an optimization problem for industrial load control. Let $\mathcal{V} = \mathcal{S} \cup \mathcal{C}$ and $\mathcal{E} = \mathcal{D} \cup \mathcal{I}$ denote the set of all nodes and the set of all edges in the graph representation of the industrial complex of interest, respectively. Here, $\mathcal{S}$ is the set of square nodes and $\mathcal{C}$ denotes the set of circle nodes. Furthermore, $\mathcal{D}$ is the set of edges that are represented with dashed lines and $\mathcal{I}$ denotes the set of edges that are represented by solid lines. Time is divided into equal length time slots. Without loss of generality, we assume that the length of each time slot is 15 minutes. The set of time slots is denoted by $\mathcal{T} = \{1, ..., T\}$, where T is the number of time slots in the scheduling horizon. For example, in case of day-ahead energy consumption scheduling, we have $T = 24 \times 4 = 96$. The per-time slot electricity consumption associated with each node i is denoted by l_i.

4.2.1 Decision Variables

For each unit $i \in \mathcal{V}$, let $x_i[t] \in \{0, 1\}$ denote whether unit i is operating during time slot $t \in \mathcal{T}$. That is, we have $x_i[t] = 1$ if unit i is 'on' during time slot t and $x_i[t] = 0$ if unit i is 'off' during time slot t. The decision variables in our proposed optimal industrial load control framework are $\boldsymbol{x} = (x_i[t],\ \forall i \in \mathcal{V},\ t \in \mathcal{T})$.

4.2.2 Objective Function

At each time slot $t \in \mathcal{T}$, the total scheduled electricity consumption of the industrial complex can be calculated as

$$\sum_{i \in \mathcal{V}} x_i[t]\, l_i. \tag{4.1}$$

Thus, the electricity cost of the complex in the scheduling horizon becomes

$$\sum_{t\in\mathcal{T}}\left(\sum_{i\in\mathcal{V}} x_i[t]\, l_i\right)\, p[t], \tag{4.2}$$

where $p[t]$ denotes the price of electricity at time slot t. The objective in our proposed optimal industrial load control framework is to minimize the expression (4.2).

4.2.3 Operation Completion Constraints

To assure completion of the operation of all units within the scheduling horizon, for each unit $i \in \mathcal{V}$, it is required that

$$\sum_{t\in\mathcal{T}} x_i[t] = a_i, \tag{4.3}$$

where $a_i = a_{i,j}$ for each $(i,j) \in \mathcal{E}$. Note that we assume all outgoing edges of each unit in the graph representation have the same weight, as is shown in Fig. 4.2.

4.2.4 Sequential Operation Constraints

Due to the inter-dependency among units, a particular unit cannot start its operation until all units that feed it finish their operations. This can be modeled mathematically if for each pair of nodes $i, j \in \mathcal{V}$ such that $(i,j) \in \mathcal{E}$, we have

$$x_j[t] \le \frac{1}{a_{i,j}} \sum_{k=1}^{t-1} x_i[k], \quad \forall t \in \mathcal{T}. \tag{4.4}$$

From (4.4), if $\sum_{k=1}^{t-1} x_i[k] < a_{i,j}$, i.e., if the operation of unit i is *not* completed before time slot t, then $x_j[t] = 0$, i.e., unit j *cannot* start its operation at time slot t. Together, constraints (4.4) for all $(i,j) \in \mathcal{E}$ will assure that the operation of unit j may start only after all its feeding units finish their operation.

4.2.5 Immediate Start Constraints

Recall from Section 4.1.2 that if an edge (i, j) is shown as a solid line in the graph representation in Fig. 4.2, then it indicates that the operation of unit j must start immediately after unit i finishes its operation. This can be modeled mathematically if for each pair of notes $i, j \in \mathcal{V}$ such that $(i, j) \in \mathcal{I}$, we have

$$x_j[t] \leq x_i[t-1] + \sum_{k=1}^{t-1} x_j[k], \quad \forall t \in \mathcal{T} \setminus \{1\}. \tag{4.5}$$

From (4.5), at each time slot $t \in \mathcal{T}$, $x_j[t]$ is nonzero only if either $\sum_{k=1}^{t-1} x_j[k] > 0$, i.e., the operation of unit j has already started, or $x_i[t-1] = 1$, i.e. unit i was operating during the last time slot. Together, constraints (4.3)-(4.5) assure that unit j starts operation as soon as the operation of unit i is complete.

4.2.6 Uninterruptible Operation Constraints

Recall that uninterruptable units are presented as square nodes in the graph representation in Fig. 4.2. For an uninterruptable unit, once the operation starts, it must continue until the operation is completed. This property can be modeled mathematically if for each node $i \in \mathcal{S}$, we have

$$x_i[t] \leq x_i[t+1] + \frac{1}{a_i} \sum_{k=1}^{t} x_i[k], \quad \forall t \in \mathcal{T} \setminus \{T\}. \tag{4.6}$$

where a_i is defined earlier in Section 4.2.3 and denotes number of time slots that unit i should operate. From (4.6), at each time slot $t \in \mathcal{T}$, $x_i[t]$ is nonzero only if either $x_i[t+1] = 1$, i.e., the operation of unit i continues in the next time slot, or $\sum_{k=1}^{t} x_i[k] = a_i$, i.e., the operation of unit i finishes by the end of the current time slot. It is worth mentioning that constraint

(4.6) is different from a partly similar constraint that was defined for uninterruptable loads in [33]. In particular, it does *not* require using any auxiliary variable.

4.2.7 Maximum Load Constraint

The total power draw of the industrial complex of interest should also be maintained below a limit at any time:

$$\sum_{i \in \mathcal{V}} l_i \, x_i[t] \leq L_{\max}, \quad \forall t \in \mathcal{T}, \tag{4.7}$$

where $L_{\max} > 0$ is set by the utility and depends on the limits of the power grid and the transmission lines in the region.

4.2.8 Optimization Problem Formulation

An optimal industrial load control can be modeled as the solution of the following optimization problem:

$$\begin{aligned} \underset{\boldsymbol{x}}{\textbf{Minimize}} \quad & \sum_{t \in \mathcal{T}} \left(\sum_{i \in \mathcal{V}} x_i[t] \, l_i \right) p[t] \\ \textbf{Subject To} \quad & (4.3) - (5.36). \end{aligned} \tag{4.8}$$

It is a *linear binary program* which can be solved using optimization software, such as MOSEK [11] and CPLEX [10].

4.3 Numerical Results

In this section, we assess our proposed industrial load control scheme for the BP refinery in Kwinana in Figs. 4.1 and 4.2. The number of time slots in the scheduling horizon

is $T = 20$, i.e. the decision horizon is five hours. The limit on total load at each time slot is $L_{\max} = 300\,kWh$.

4.3.1 Optimal Schedule

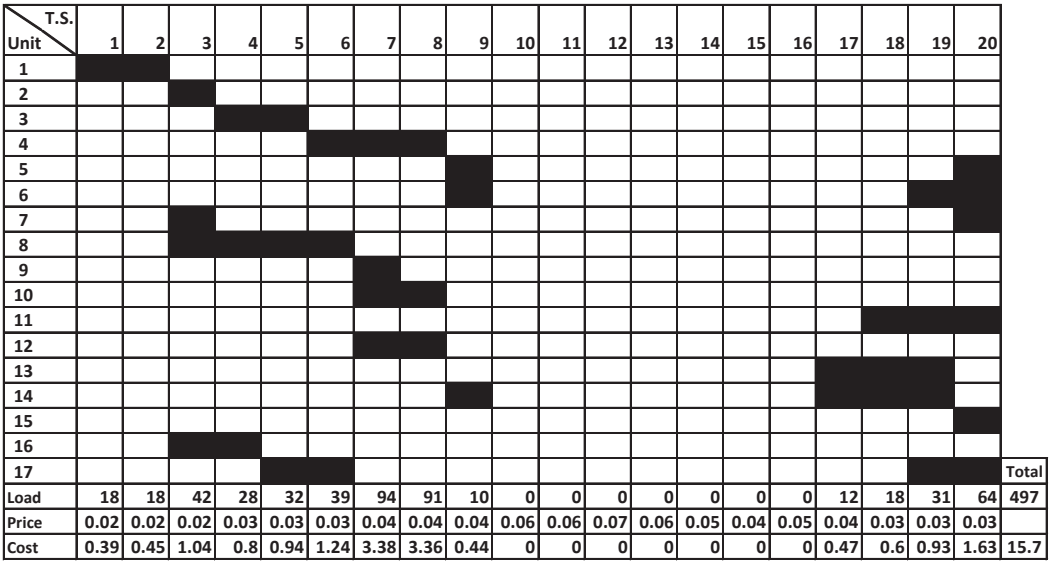

T.S. / Unit	1	2	3	4	5	6	7	8	9	10	11	12	13	14	15	16	17	18	19	20	
1	■	■																			
2			■																		
3				■	■																
4						■	■	■													
5									■											■	
6									■										■	■	
7			■																	■	
8			■	■	■	■															
9							■														
10							■	■													
11																		■	■	■	
12							■	■													
13																	■	■	■		
14									■								■	■	■		
15																				■	
16			■	■																	
17					■	■													■	■	Total
Load	18	18	42	28	32	39	94	91	10	0	0	0	0	0	0	0	12	18	31	64	497
Price	0.02	0.02	0.02	0.03	0.03	0.03	0.04	0.04	0.04	0.06	0.06	0.07	0.06	0.05	0.04	0.05	0.04	0.03	0.03	0.03	
Cost	0.39	0.45	1.04	0.8	0.94	1.24	3.38	3.36	0.44	0	0	0	0	0	0	0	0.47	0.6	0.93	1.63	15.7

Figure 4.4: Optimal energy consumption schedule based on the proposed scheme.

The optimal load schedule is shown in Fig. 4.4. It is calculated based on the solution of problem (4.8). We can see that although optimal scheduling consumes the same amount of electricity during scheduling horizon as the two examples of Section 4.1.3, it results in noticeably lower electricity cost.

To make it visual, price function and the load profile of examples 1 and 2 and optimal scheduling is shown in Fig. 4.5. As can be seen in Fig. 4.5, most of the load of example 1 is scheduled during higher price time slots whereas load of example 2 is scheduled during lower price time slots and consequently example 2 has a lower cost than example

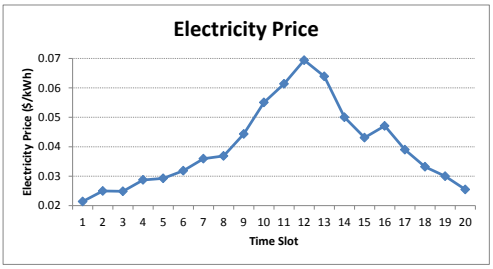

(a) Price function

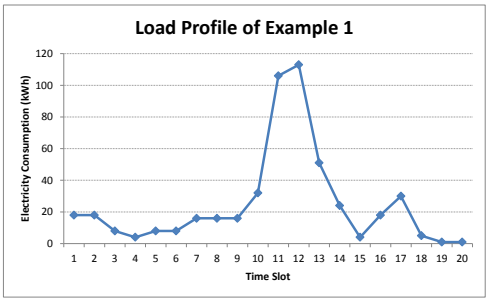

(b) Load profile of example 1

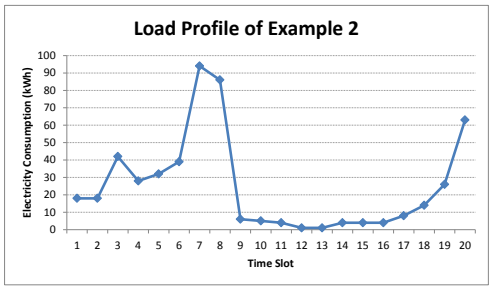

(c) Load profile of example 2

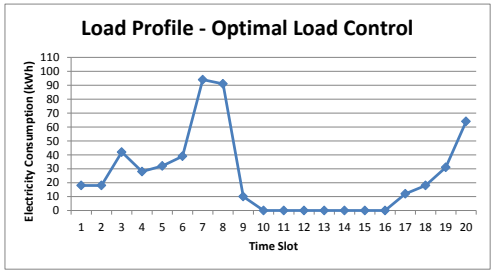

(d) Load profile of optimal schedule

Figure 4.5: Price function and load profiles of examples 1 and 2 and optimal schedule

1. On the other hand, the load of optimal schedule has the lowest electricity cost possible during the scheduling horizon among all feasible scheduling.

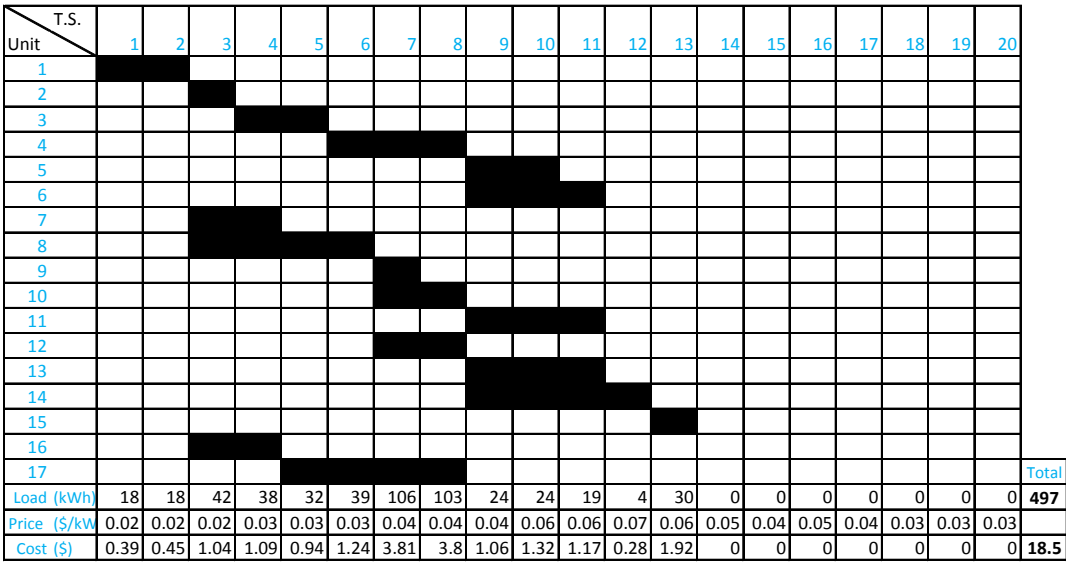

T.S. / Unit	1	2	3	4	5	6	7	8	9	10	11	12	13	14	15	16	17	18	19	20	
1	■	■																			
2			■																		
3				■	■																
4						■	■	■													
5									■	■											
6									■	■	■										
7			■	■																	
8			■	■	■	■															
9							■														
10							■	■													
11									■	■	■										
12							■	■													
13									■	■	■										
14									■	■	■	■									
15													■								
16			■	■																	
17					■	■	■	■													Total
Load (kWh)	18	18	42	38	32	39	106	103	24	24	19	4	30	0	0	0	0	0	0	0	**497**
Price ($/kW	0.02	0.02	0.02	0.03	0.03	0.03	0.04	0.04	0.04	0.06	0.06	0.07	0.06	0.05	0.04	0.05	0.04	0.03	0.03	0.03	
Cost ($)	0.39	0.45	1.04	1.09	0.94	1.24	3.81	3.8	1.06	1.32	1.17	0.28	1.92	0	0	0	0	0	0	0	**18.5**

Figure 4.6: Scheduling in minimum number of time slots (i.e. no scheduling)

Next, we repeat the analysis for 100 different pricing scenarios, based on the day-ahead price profiles in [34]. The results are shown in Fig. 4.7, where we compare our optimal load control approach with a base method shown in Fig. 4.6 that schedules the operation of each unit with no interruption and as soon as all its feeding units finish their operations. At every pricing scenario, our optimal scheduling cost is lower. On average, optimal load control can reduce the cost by over 14%.

4.3.2 Impact of L_{max}

Fig. 4.8 shows impact of L_{max} (maximum load allowed per time slot) on optimal cost. It can be seen that optimal cost is a nonincreasing function of L_{max}. This is because

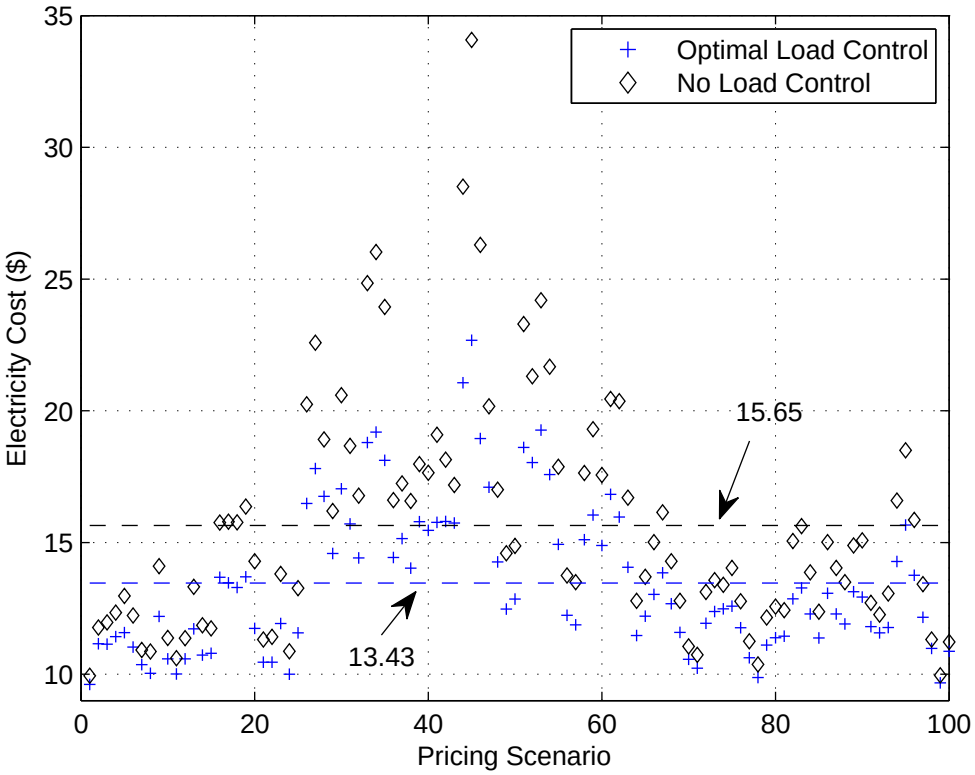

Figure 4.7: Reducing electricity cost via optimal load control for 100 different price scenarios.

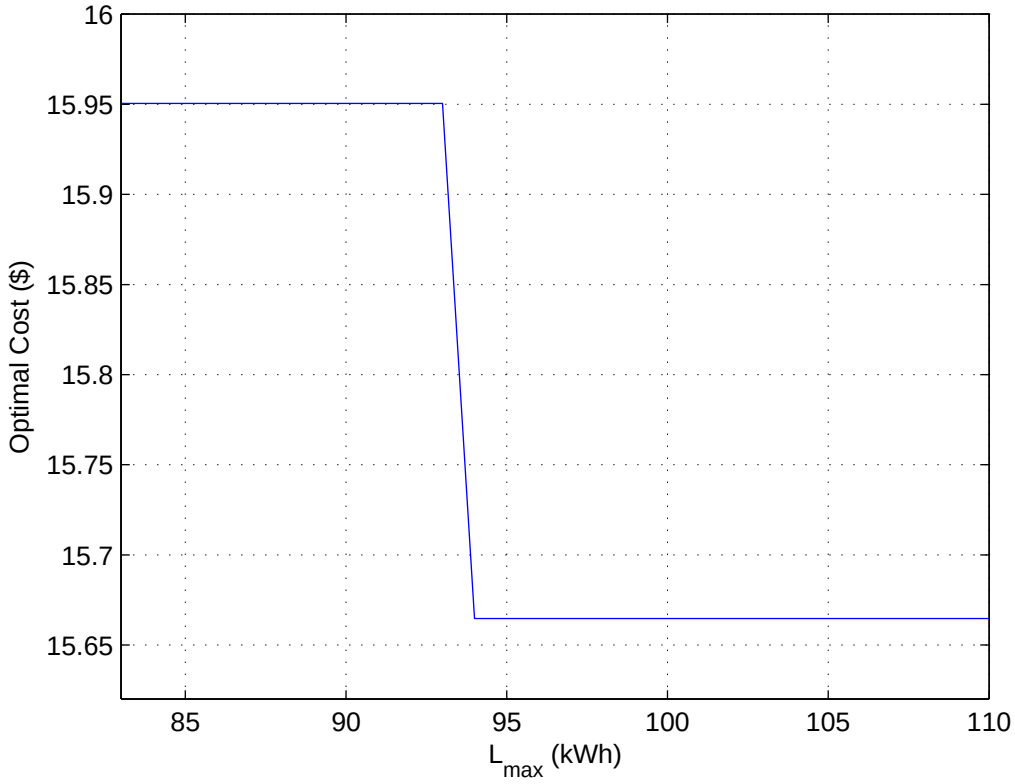

Figure 4.8: Impact of L_{max} on optimal electricity cost

as value of L_{max} increases, scheduler has more flexibility to schedule the units which will result in lower or no change in cost. In Fig. 4.8, the minimum value of L_{max} is 83 kWh since units 9, 10, and 12 should be scheduled at the same time slot (as soon as unit 8 finishes its operation). Also optimal cost is constant for any $L_{max} \geq 94$ kWh since for optimal schedule shown in Fig. 4.4 the largest load scheduled in a time slot is 94 kWh.

4.3.3 Changing the Decision Horizon

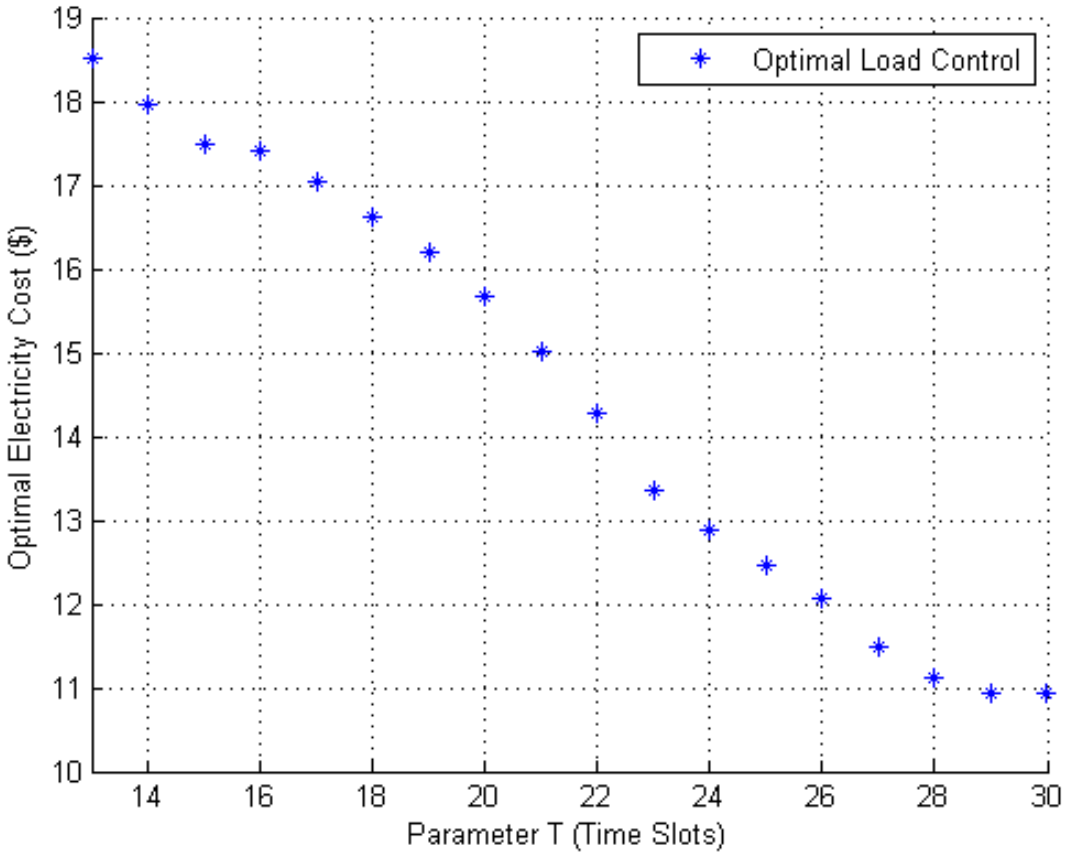

Figure 4.9: Impact of parameter T on optimal electricity cost.

The impact of changing parameter T on electricity cost is shown in Fig. 4.9. We can see that the optimal cost decreases or does not change as T increases. This is because a higher T indicates more time flexibility. Note that parameter T is lower bounded by 13 time slots, which is the minimum number of time slots required to finish the operation of all units.

4.3.4 Units Types and Edges Types

In general, interruptable units (i.e., circle nodes) and non-immediate dependencies (i.e., dashed lines) cause more flexibility in load scheduling and consequently lower electricity cost. An example is shown in Fig. 4.10. We can see that, as we increase the number of uninterruptable units (and accordingly decrease the number of interruptable units), problem (4.8) will face more restrictive constraints that may lead to increasing the electricity cost associated with the industrial complex.

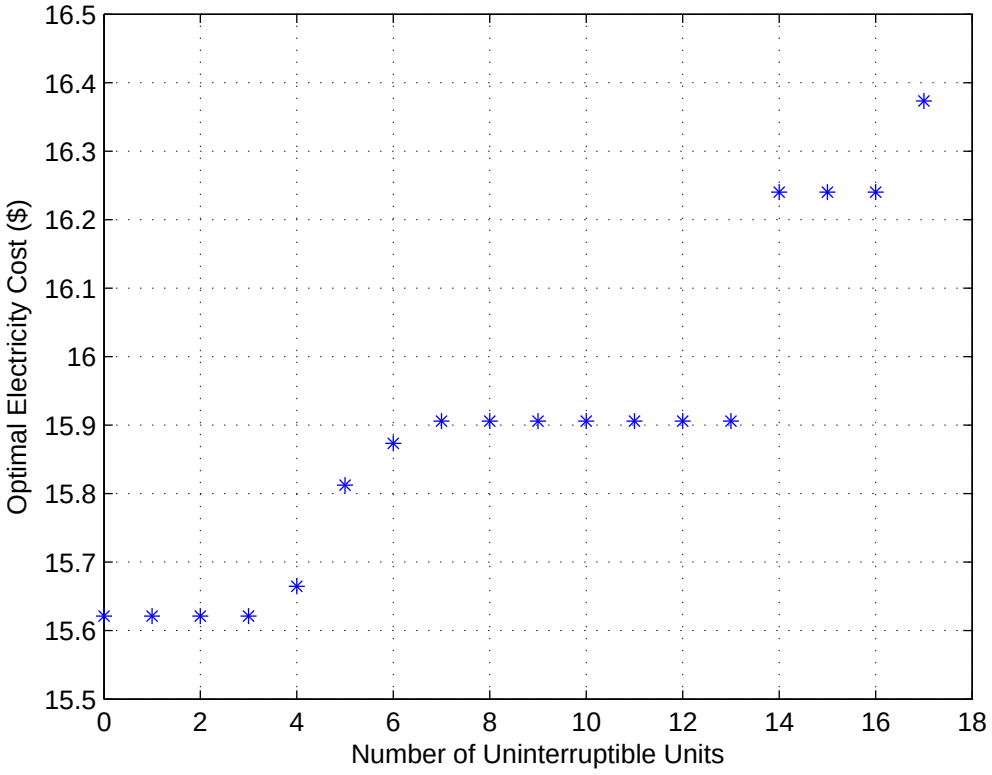

Figure 4.10: Impact of number of uninterruptible units on optimal electricity cost

Chapter 5

Comprehensive Industrial Load Control: A Case Study for Steel Industry

In this chapter, a more comprehensive industrial load control formulation is proposed and amount of material processed by a unit is included as a decision variable. Here an industrial unit takes different amount of material at each cycle and its electricity load has an affine relationship with the amount of material processed. The optimization-based industrial load control framework is proposed under different smart pricing methods in form of a tractable linear mixed-integer program. Behind-the-meter battery and renewable generation is considered. Case studies are presented in form of an illustrative example and also a steel mill industry. The major contents of this section is taken from [2].

The contributions in this chapter are summarized as follows:

- We take several industrial load details into consideration, including those that do not appear in residential or commercial load control problems. For example, industrial units are highly inter-dependent and must follow a certain operational sequence. The operation of certain industrial units may span across multiple days. Furthermore, in industries that involve process control, energy management is often coupled with material flow management.

- Operation under different smart pricing scenarios are considered: day-ahead pricing, time-of-use pricing, peak pricing, inclining block rates, and critical peak pricing. The use of behind-the-meter renewable generation and energy storage are also taken into consideration.

- The formulated industrial load control optimization problem is a tractable linear mixed-integer program.

- Case studies include an illustrative example and also a practical scenario based on a steel mill industry model.

5.1 Industrial Units as Building Blocks In An Industrial Load System

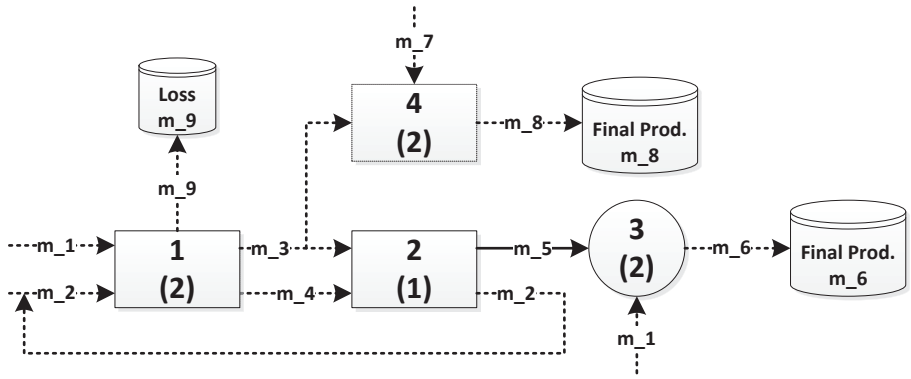

(a)

(b)

Figure 5.1: An *industry* is modeled as a collection of interacting industrial units: (a) An example industry with four units and two final products. (b) Each unit is identified by its material and energy inputs and outputs, its emission and waste, and its internal operation details, e.g., whether it is interruptible.

Consider a complex industrial system, such as the one in Fig. 5.1(a). One can model this system as a combination of several industrial units of different sizes and types that work together to produce one or multiple final products. To model each unit, we need to first identify its inputs and outputs both in terms of material and energy, as shown in Fig. 5.1(b). We are particularly interested in the electricity energy inputs to industrial units to, e.g., run electric boilers, create electric arc, run electric motors, etc. Output energy, while

not common for most units, is any *usable* energy form as a *by-product*.

The output material from one unit is often fed to another unit as input to go through a *multi-stage processing chain* before a final product is produced. As an example, in Fig. 5.1(a), we can identify two processing chains $1 \rightarrow 2 \rightarrow 3$ and $1 \rightarrow 4$ to produce final products m_6 and m_8, respectively. The raw materials are marked as m_1, m_2, and m_7. The units in a processing chain may or may not work simultaneously. However, it is always necessary to have enough input materials available at each unit, before it can start a new batch processing cycle.

Suppose time is divided into equal time slots, where each time slot is modeled by its *beginning* time. The numbers in parentheses inside each unit in Fig. 5.1(a) shows the number of time slots that the unit must operate to finish *one* batch cycle. Unit 3 is an *interruptible* load and its represented by a *circle*. If needed, its operation can be stopped in the middle of a batch cycle and restored later. In contrast, units 1, 2, and 4 are represented by *rectangles* because they are *uninterruptible*. The flow of material m_5 from unit 2 to unit 3 is shown with a *solid* line to highlight that due to its pressure, temperature, or other characteristics, material m_5 must be processed by unit 3 as soon as it is produced by unit 2. In contrast, a material flow with *dashed* line represents a material that does not have to be processed immediately; hence, it can be stored and used at a later time. Material m_2 is a usable *by-product* of unit 2 that is fed back to unit 1. Also note that materials m_1 and m_3 are consumed by multiple units. Finally, each unit may undergo *different number of cycles*. For example, unit 1 may undergo 3 cycles while units 2, 3, and 4 may undergo 2 cycles only.

5.2 Problem Formulation

One can *shape* the electric load profile of an industrial load by adjusting the *operational schedule* of its batch processing units subject to their operational needs and inter-operational sequences. In this section, we formulate the design objective, decision variables, and constraints in an optimal ILC problem.

5.2.1 Objective Function

The primary goal of any industry is to maximize its profit, i.e., its *revenue* minus *cost*. On one hand, revenue depends on the amount and sale price of each final product. On the other hand, cost depends on the amount and purchase price of raw materials and also the operational cost of industrial units, including their cost of electricity. Therefore, we have

$$\text{Profit} = \text{Revenue} - \text{Cost}, \tag{5.1}$$

where

$$\text{Revenue} = \sum_{f \in \mathcal{F}} m_f[T] p_f, \tag{5.2}$$

and

$$\begin{aligned} \text{Cost} = & \sum_{r \in \mathcal{R}} \left(m_r[0] - m_r[T] \right) p_r \\ & + \sum_{t=1}^{T} \sum_{k \in \mathcal{K}} m_k[t] \gamma_k + C_{fixed} + C_{elct}. \end{aligned} \tag{5.3}$$

The first term in (5.3) is the total cost of raw materials consumed during the scheduling horizon. The second term is the total cost of storing materials of any type. The third term is any fixed cost that does not depend on our decision variables, e.g., cost of labor,

facility, etc. Finally, and most importantly, the fourth term is the *cost of electricity*, which we explain next.

5.2.2 Cost of Electricity

The cost of electricity depends on both the electric load profile and the pricing method used by the utility company.

Day-Ahead Pricing (DAP)

This pricing method is used, e.g., by Ameren Inc. in Illinois [34]. In DAP, the utility releases the hourly prices for the next day on a daily basis. Let $p[t]$ \$/kWh denote the day-ahead price of electricity at time slot t. Also let $L[t]$ denote the *total* power consumption at the industrial complex of interest at time slot t. We have:

$$C_{elct} = \sum_{t=1}^{T} L[t]p[t], \tag{5.4}$$

where T is the scheduling horizon.

Time-of-Use Pricing (ToUP)

This pricing method is used, e.g., by Pacific Gas & Electric in California for commercial and industrial users [35]. In ToUP, there are multiple rate periods as *on-peak*, *mid-peak*, and *off-peak* hours. Prices are usually fixed over a season. Mathematically, ToUP is a special case of DAP; therefore, the cost of electricity when ToUP is used is formulated similar to the expression in (5.4).

Peak Pricing (PP)

This pricing method is used, e.g., by Riverside Public Utilities in California [36]. It usually has two components: *usage charge* and *peak demand charge*. Usage charge is based on flat or time-of-use rates. It can be modeled as in (5.4). Peak demand charge is rather based on the consumer's daily or monthly peak load. It is calculated by measuring electricity usage at the hour of the day or month during which the consumer's load is at its highest amount. The peak price, denoted by p_{pd} \$/kWh, is usually much higher than the prices that are used to calculate the usage charge. That is, $p_{pd} \gg p[t]$ for all $t \in \mathcal{T}$. As a result, PP can encourage users to consume electricity more *uniformly* during the day in order to improve the *load factor*. The cost of electricity when PP method is used can be calculated as

$$C_{elct} = \sum_{t=1}^{T} L[t]p[t] + \left(\underset{t}{max}\, L[t]\right) p_{pd}. \tag{5.5}$$

Inclining Block Rates (IBR)

This pricing method is another way to encourage balanced load profiles. It also encourages energy conservation. It is offered, e.g., by British Columbia Hydro in Canada to industrial users [18]. In IBR pricing, beyond a certain load *threshold*, the price increases to a higher value. In a typical two-tier IBR model, we have [18]:

$$p[t] = \begin{cases} p_{bl}[t] & \text{if } L[t] \leq L_0[t], \\ \\ p_{hl}[t] & \text{if } L[t] > L_0[t], \end{cases} \tag{5.6}$$

where $p_{bl}[t]$, $p_{hl}[t]$, and $L_0[t]$ are the price parameters at time t. If $L[t] \leq L_0[t]$, then the cost of electricity at time t becomes

$$C_{elct}[t] = p_{bl}[t]L[t]. \tag{5.7}$$

Otherwise, i.e., if $L[t] > L_0[t]$, we have

$$C_{elct}[t] = p_{bl}[t]L_0[t] + (L[t] - L_0[t])\, p_{hl}[t]. \tag{5.8}$$

The total cost of electricity during an interval of interest $[1, T]$ under IBR pricing is calculated as $C_{elct} = \sum_{t=1}^{T} C_{elct}[t]$.

Critical Peak Pricing (CPP)

This pricing method is used, e.g., by Fort Collins Utilities in Fort Collins, CO [37]. In CPP, there is an additional charge during the hours where the utility experiences spikes in the total load demand in its service territory. Since CPP depends on the *combined behavior* of all consumers, individual customers are unaware of its happening time. Therefore, utilities send *warnings* from 5 minutes to 24 hours in advance to inform users about the occurrence of an upcoming critical peak hour. The exact setup of CPP may vary in different places. In this paper, we assume that the CPP price p_{cp} \$/kWh and the start and duration of each critical peak hour are announced as part of the warning signal sent by the utility. Following the analysis of historical CPP warnings in [38], we assume that warnings accurately identify the critical peak hour, i.e., no CPP false alarm may be sent to consumers.

Similar to PP, CPP is usually combined with usage charges. The cost of electricity

under CPP pricing methods becomes

$$\sum_{t=1}^{t_{beg}-1} L[t]p[t] + \sum_{t=t_{beg}}^{t_{end}} L[t]p_{cp} + \sum_{t=t_{end}+1}^{T} L[t]p[t], \tag{5.9}$$

where t_{beg} and t_{end} denote the beginning and the end of the critical peak time frame, where $t_{beg} < t_{end}$. The CPP price is usually much higher than the regular usage price and even peak price. As reported in [38], when CPP is used, at least 23% of the cost of electricity comes from the CPP charges.

5.2.3 Decision Variables

The decision variables in our proposed problem formulation and the range of the values that they can take are as follows:

$$\begin{aligned}
&s_i[t] \in \{0, 1, 2, ...\}, && \forall i, \forall t, \\
&e_i[t] \in \{0, 1, 2, ...\}, && \forall i, \forall t, \\
&x_i[t] \in \{0, 1\}, && \forall i, \forall t, \\
&u_i[t] \in \{0\} \cup [\alpha_i, \beta_i], && \forall i, \forall t, \\
&y_i[t] \geq 0, && \forall i, \forall t, \\
&m_k[t] \in [0, \eta_k], && \forall k, \forall t, \\
&l_i[t] \geq 0, && \forall i, \forall t.
\end{aligned} \tag{5.10}$$

The definitions of the above variables are given in the nomenclature. Next, we explain these variables and their relationship.

5.2.4 Batch Cycle's Start and End Time Constraints

As listed in the nomenclature, $s_i[t]$ denotes the number of unit i's batch cycles that started before or at time slot t. Similarly, $e_i[t]$ denotes the number of unit i's batch cycles that ended before or at time slot t. These two sets of variables are defined in order to keep track of the start time and the end time of each batch cycle in each unit. By definition, we have:

$$0 \leq s_i[t] - s_i[t-1] \leq 1, \quad \forall i, \forall t, \tag{5.11}$$

$$0 \leq e_i[t] - e_i[t-1] \leq 1, \quad \forall i, \forall t, \tag{5.12}$$

where for each unit i the initial condition is defined as $s_i[0] = e_i[0] = 0$. If at a time slot t we have $s_i[t] - s_i[t-1] = 1$, then unit i has started a *new* cycle at time slot t and if $e_i[t] - e_i[t-1] = 1$, then unit i has finished a cycle at time slot t. Since a unit may not start a new cycle unless its current cycle has ended, the following inequalities must hold:

$$0 \leq s_i[t] - e_i[t] \leq 1, \quad \forall i, \forall t. \tag{5.13}$$

Note that, if $s_i[t] - e_i[t] = 0$, then $s_i[t] = e_i[t]$, i.e., all batch cycles that started before or at time slot t also finished before or at time slot t. If $s_i[t] - e_i[t] = 1$, then the current cycle is *in process* and it has not finished yet. The following terminal conditions also need to hold in order to assure that all batch cycles for all units end before the end of the decision horizon:

$$s_i[T] = e_i[T], \quad \forall i. \tag{5.14}$$

Last but not least, we need to enforce the following terminal constraint on $x_i[t]$ for each unit i to complement the constraints in (5.14) such that no unit operates at the last time

slot $t = T$ and that time is used only for delivering final products:

$$x_i[T] = 0, \quad \forall i. \tag{5.15}$$

5.2.5 Batch Cycle's Operational Constraints

Next, we need to relate variables $s_i[t]$ and $e_i[t]$ to $x_i[t]$ which is the primary variable to control the operation of each unit i. Let parameter a_i denotes the number of time slots that unit i must operate to finish one batch cycle. Then

$$s_i[t] = \begin{cases} 0, & \text{if } \sum_{j=1}^{t} x_i[j] = 0 \\ 1, & \text{if } 1 \leq \sum_{j=1}^{t} x_i[j] \leq a_i \\ 2, & \text{if } a_i + 1 \leq \sum_{j=1}^{t} x_i[j] \leq 2a_i \\ \vdots & \end{cases} \quad \forall i, \forall t \tag{5.16}$$

and

$$e_i[t] = \begin{cases} 0, & \text{if } 0 \leq \sum_{j=1}^{t} x_i[j] \leq a_i - 1 \\ 1, & \text{if } a_i \leq \sum_{j=1}^{t} x_i[j] \leq 2a_i - 1 \\ 2, & \text{if } 2a_i \leq \sum_{j=1}^{t} x_i[j] \leq 3a_i - 1 \\ \vdots & \end{cases} \quad \forall i, \forall t \tag{5.17}$$

After reordering the terms, we can replace (5.16) and (5.17) with the following equivalent but more tractable constraints:

$$(s_i[t] - 1)a_i + 1 \leq \sum_{j=1}^{t} x_i[j] \leq s_i[t]a_i, \quad \forall i, \forall t, \tag{5.18}$$

$$e_i[t]a_i \leq \sum_{j=1}^{t} x_i[j] \leq (e_i[t] + 1)a_i - 1, \quad \forall i, \forall t. \tag{5.19}$$

5.2.6 Input and Output Timing Constraints

For a unit that operates in batch cycles, it may import its input materials only at the *beginning* of its batch cycles. Recall from Section 5.2.4 that time slot t is the beginning of a batch cycle for unit i if and only if $s_i[t] - s_i[t-1] = 1$. Therefore, to assure the right timing of material entrance to unit i, the amount of materials entering unit i at time slot t denoted by $u_i[t]$ must satisfy $u_i[t] \in [\alpha_i, \beta_i]$ if $s_i[t] - s_i[t-1] = 1$, and $u_i[t] = 0$ if $s_i[t] - s_i[t-1] = 0$. This can be equivalently expressed in form of the following linear inequality constraints:

$$u_i[t] \geq (s_i[t] - s_i[t-1])\,\alpha_i, \quad \forall i, \forall t, \tag{5.20}$$

$$u_i[t] \leq (s_i[t] - s_i[t-1])\,\beta_i, \quad \forall i, \forall t. \tag{5.21}$$

Similarly, each unit may export its output materials only at the *end* of its batch cycles. Recall from Section 5.2.4 that time slot t is the end of a batch cycle for unit i if and only if $e_i[t] - e_i[t-1] = 1$. Also recall that all events happen at the beginning of a time slot and hence, it is assumed that output materials are produced at the beginning of the next time slot when a cycle ends. Therefore, to assure the right timing of material exit from unit i, the amount of materials exiting from unit i at time slot t denoted by $y_i[t]$ must satisfy $y_i[t+1] \geq 0$ if $e_i[t] - e_i[t-1] = 1$, and $y_i[t+1] = 0$ if $e_i[t] - e_i[t-1] = 0$ for all $t \in [1, T)$. This can be equivalently expressed in form of the following linear inequality constraints:

$$y_i[t+1] \geq 0, \quad \forall i, \forall t < T, \tag{5.22}$$

$$y_i[t+1] \leq \Omega\,(e_i[t] - e_i[t-1]), \quad \forall i, \forall t < T, \tag{5.23}$$

where $\Omega \gg 0$ is a large enough number. Finally, the following constraints assure that no

material may leave any unit at the very beginning of the decision process, i.e., at time $t = 1$:

$$y_i[1] = 0, \quad \forall i. \tag{5.24}$$

5.2.7 Material Balance and Proportionality Constraints

The requirement for material balance in each unit is defined as the equality between the total amount of input materials that enter the unit at the beginning of each batch cycle and the total amount of output materials, including any waste, that leave the unit at the end of the same batch cycle. Since materials enter a unit only at the beginning of batch cycles and leave the unit only at the end of batch cycles, the above definition can be mathematically expressed in form of the following constraints:

$$\begin{aligned} &\sum_{j=1}^{t} y_i[j+1]\left(e_i[j] - e_i[j-1]\right) \\ &= \sum_{j=1}^{t} u_i[j]\left(e_i[j] - e_i[j-1]\right), \quad \forall i, \forall t. \end{aligned}$$

The above constraints require that by the end of each batch cycle, the total material that enters the unit must match the total material that leaves the unit. These nonlinear constraints can be replaced by the following equivalent linear constraints:

$$\begin{aligned} 0 &\leq \sum_{j=1}^{t} u_i[j] - \sum_{j=1}^{t} y_i[j+1] \\ &\leq \Omega\left(1 - e_i[t] + e_i[t-1]\right), \quad \forall i, \forall t < T, \end{aligned} \tag{5.25}$$

Besides material balance in each unit, material balance should hold also across all units. That is, we need to have:

$$m_k[t] = m_k[t-1] + \sum_{i \in \mathcal{I}_k^{out}} q_i^k y_i[t] - \sum_{i \in \mathcal{I}_k^{in}} r_i^k u_i[t], \quad \forall k, \forall t, \tag{5.26}$$

where $m_k[0]$ is the amount of material k that is initially available in the storage. Note that, for each industrial unit i, we have $\sum_{k\in\mathcal{K}} r_i^k = 1$ and $\sum_{k\in\mathcal{K}} q_i^k = 1$. Constraint (5.26) is valid for all types of materials including non-storable materials.

5.2.8 Material Storage Constraints

The amount of each material k stored at any time may not exceed the capacity of its corresponding storage tank η_k. Also the amount of each material k stored at any time cannot be negative. These constraints can be formulated as

$$0 \leq m_k[t] \leq \eta_k, \quad \forall k, \forall t. \tag{5.27}$$

Next, recall from Section 5.1 that certain materials cannot be stored. Rather they must be immediately sent to the next unit along the processing chain. Let $\mathcal{K}_{imd}$ denote the set of materials with such requirements. We need to have:

$$\eta_k = 0, \quad \forall k \in \mathcal{K}_{imd}. \tag{5.28}$$

From (5.28) and (5.27), we have $m_k[t] = 0$, $\forall k \in \mathcal{K}_{imd}$ and $\forall t$.

We also need specific constraints with respect to the storage of final products. Without loss of generality, we assume that storage facilities of final products are initially empty and final products of each cycle are accumulated until the end of scheduling horizon. Therefore, $m_f[T]$ indicates the sum of final products f that are produced during the load scheduling horizon. The following captures the production requirement:

$$m_f[T] \geq \phi_f, \quad \forall f \in \mathcal{F}. \tag{5.29}$$

5.2.9 Constraints for Uninterruptible Units

While there exist industrial units, e.g., in the automotive industry, whose operations can be interrupted and later restored, there are also units, e.g., in chemical industries, whose operations *cannot* be interrupted. Once an uninterruptible unit starts a batch cycle, it may not stop operation until it finishes its current batch cycle. Mathematically, this means that if $s_i[t]-s_i[t-1]=1$, then we must have $x_i[t]=x_i[t+1]=\cdots=x_i[t+a_i-1]=1$. To model this mathematically, first, we note that a batch cycle for an uninterruptable load may start anywhere between time slots $t=1$ and $t=T-a_i+1$; otherwise, the batch cycle does not finish by the end of the load scheduling horizon at time $t=T$. Therefore, in order to assure the proper operation of an uninterruptable unit, the following constraints must hold for any $j=0,1,\ldots,a_i-1$:

$$s_i[t]-s_i[t-1]\leq x_i[t+j], \forall i\in\mathcal{I}_{unt}, \forall t\in[1,T-j]. \tag{5.30}$$

Note that, if at a time slot t, we have $s_i[t]-s_i[t-1]=1$, then (5.30) becomes $1\leq x_i[t+j]$, for all $j=0,1,\ldots,a_{i-1}$. That is, $x_i[t]=x_i[t+1]=\ldots=x_i[t+a_i-1]=1$.

5.2.10 Electricity Consumption Constraints

In general, the amount of power consumption at an industrial unit depends on whether the unit is *operating* or it is on *stand-by* and also the amount of material that is loaded into the unit during its operation. In this regard, we can model

$$l_i[t]=\begin{cases} l_i^{min} & \text{if } x_i[t]=0 \\ c_iM_i[t]+d_i & \text{if } x_i[t]=1 \end{cases} \quad \forall i,\forall t, \tag{5.31}$$

where the notations are defined in the nomenclature and

$$M_i[t] = \sum_{j=1}^{t} u_i[j] - \sum_{j=1}^{t} y_i[j] \tag{5.32}$$

denotes the total amount of all materials that is inside unit i at time slot t. We can replace (5.31) with the following constraints:

$$l_i[t] \geq l_i^{min}, \quad \forall i, \forall t, \tag{5.33}$$

$$l_i[t] \geq c_i M_i[t] + d_i - \Omega\left(1 - x_i[t]\right), \quad \forall i, \forall t, \tag{5.34}$$

where Ω is a large enough number. Assuming that for each unit i, we have $l_i^{min} \leq d_i$, we can explain (5.33) and (5.34) as follows. If $x_i[t] = 1$, then (5.33) and (5.34) reduce to $l_i[t] \geq c_i M_i[t] + d_i$. And if $x_i[t] = 0$, then (5.33) and (5.34) reduce to $l_i[t] \geq l_i^{min}$.

Based on the above explanations, the total power consumption across all units in the industrial complex becomes:

$$L[t] = \sum_{i \in \mathcal{V}} l_i[t] + l_{back}[t], \tag{5.35}$$

where $l_{back}[t]$ is known and denotes the background load which includes the facility loads (such as lighting and HVAC) and non-controllable loads (such as units that operate continuously). Recall that this amount has to be upper bounded:

$$L[t] \leq L_{max}, \quad \forall t, \tag{5.36}$$

where L_{max} is determined based on the type of the meter and electric feeder that the industrial complex is connected to.

5.2.11 Profit Maximization Problem

We are now ready to formulate the following profit maximization problem for the purpose of energy consumption scheduling for industrial complexes and industrial processes:

$$\underset{(5.10)}{\textbf{Maximize}} \quad \sum_{f\in\mathcal{F}} m_f[T]\, p_f - \sum_{r\in\mathcal{R}} \left(m_r[0] - m_r[T]\right)\, p_r - \sum_{t=1}^{T}\sum_{k\in\mathcal{K}} m_k[t]\, \gamma_k - C_{fixed} - C_{elct} \tag{5.37}$$

$$\textbf{Subject to } (5.11)-(5.15), (5.18)-(5.30), (5.33)-(5.34), (5.36).$$

Note that, depending on the exact pricing model being applied, we replace C_{elct} in (7.4) with one of the electricity cost models in (5.4) to (5.9). However, regardless of the choice of the electricity cost model, the optimization problem in (7.4) is either a *mixed integer linear program* (MILP) or it can be easily converted to an MILP; therefore, it can be solved efficiently and in a timely fashion using MILP optimization software, such as MOSEK [11] and CPLEX [10].

5.2.12 Behind-the-Meter Batteries and Renewable Generators

The problem formulation in (7.4) can easily be modified to also include batteries and renewable generators. To include batteries in the ILC problem, we introduce three new variables: $l_{ch}[t]$ and $l_{dch}[t]$ to indicate the charge and discharge rates of the battery system at slot time t, respectively, and $b[t] \in \{0, 1\}$ to indicate if the battery is charged or discharged at time slot t. If $b[t] = 1$, then the battery is charged at time slot t, and if $b[t] = 0$, then the battery is discharged. It is required that

$$0 \le l_{ch}[t] \le b[t] l_{ch}^{max}, \quad \forall t, \tag{5.38}$$

$$0 \leq l_{dch}[t] \leq (1 - b[t]) l_{dch}^{max}, \quad \forall t, \tag{5.39}$$

where l_{ch}^{max} and l_{dch}^{max} denote the maximum charge rate and the maximum discharge rate of the batteries, respectively. Since the batteries cannot be discharged if they are empty and they cannot be charged if they are full, the following constraints are also needed in the problem formulation:

$$0 \leq B^{init} + \sum_{j=1}^{t} (\mu \, l_{ch}[j] - \theta \, l_{dch}[j]) \leq B^{full}, \quad \forall t, \tag{5.40}$$

where B^{init} and B^{full} denote the initial charge level and the full charge capacity of the battery system, respectively. Here, $\mu \leq 1$ and $\theta \geq 1$ denote the efficiency of the battery system during charge and discharge, respectively.

Besides adding constraints (5.38)-(5.40) to the the problem in (7.4), we also need to slightly revise the load models in (5.35) in order to incorporate the impact of adding on-site batteries:

$$L[t] = \sum_{i \in \mathcal{V}} l_i[t] + l_{back}[t] + l_{ch}[t] - l_{dch}[t], \quad \forall t. \tag{5.41}$$

In general, $L[t]$ in (5.41) may take both positive and negative values. In particular, $L[t]$ can be negative if the rate at which the battery is discharged at time t is higher than the total power consumption at the industrial complex at time t. If $L[t] < 0$, then it means that the industrial complex is injecting power back to the grid. Depending on the policies set forth by the regional utility company that feeds the industrial complex, a back injection power may or may not be allowed, as some protection devices on distribution systems may not support back injections. In that case, it is required to also add the following constraints

into the problem formulation:

$$L[t] \geq 0, \quad \forall t. \tag{5.42}$$

Finally, suppose the industrial complex is equipped with local renewable generator and renewable generator outputs are predicted accurately at each time slot. In that case, equation (5.41) should be slightly revised as follows:

$$L[t] = \sum_{i \in \mathcal{V}} l_i[t] + l_{back}[t] + l_{ch}[t] - l_{dch}[t] - l_{slr}[t], \quad \forall t, \tag{5.43}$$

where $l_{slr}[t]$ is the expected available solar energy at time t.

5.3 Case Studies

5.3.1 Illustrative Example

Consider the industry in Fig. 5.1(a), where the parameters of industrial units are as in Table 5.1. Here, α_i and β_i are in kg, c_i is in kWh/kg, and d_i is in kWh. The storage capacity is 1000 kg for all materials, except for material 5 which is zero. The initial amount of the nine materials are 1000, 500, 0, 0, 0, 0, 1000, 0, 0 kg. The unit price for raw materials 1, 2, and 7 are 10, 5, and 20 \$/kg, respectively. The unit price for final products 6, 8, and 9, are 50, 100, and 0 \$/kg, respectively. The minimum needed final products are 10, 10, and 0 kg, respectively. Background load is zero at all time slots, and $L_{max} = 5 \times 10^5$ kWh. The ILC horizon is $T = 15$ time slots.

Table 5.1: Parameters in the illustrative example

i	a_i	(α_i, β_i)	r_i^k	q_i^k	(c_i, d_i)
1	2	(40,200)	0.6,0.4	0.7,0.2,0.1	(5,1)
2	1	(30,150)	0.3,0.7	0.2,0.8	(5,1)
3	2	(20,100)	0.5,0.5	1	(5,1)
4	2	(10,50)	0.2,0.8	1	(5,1)

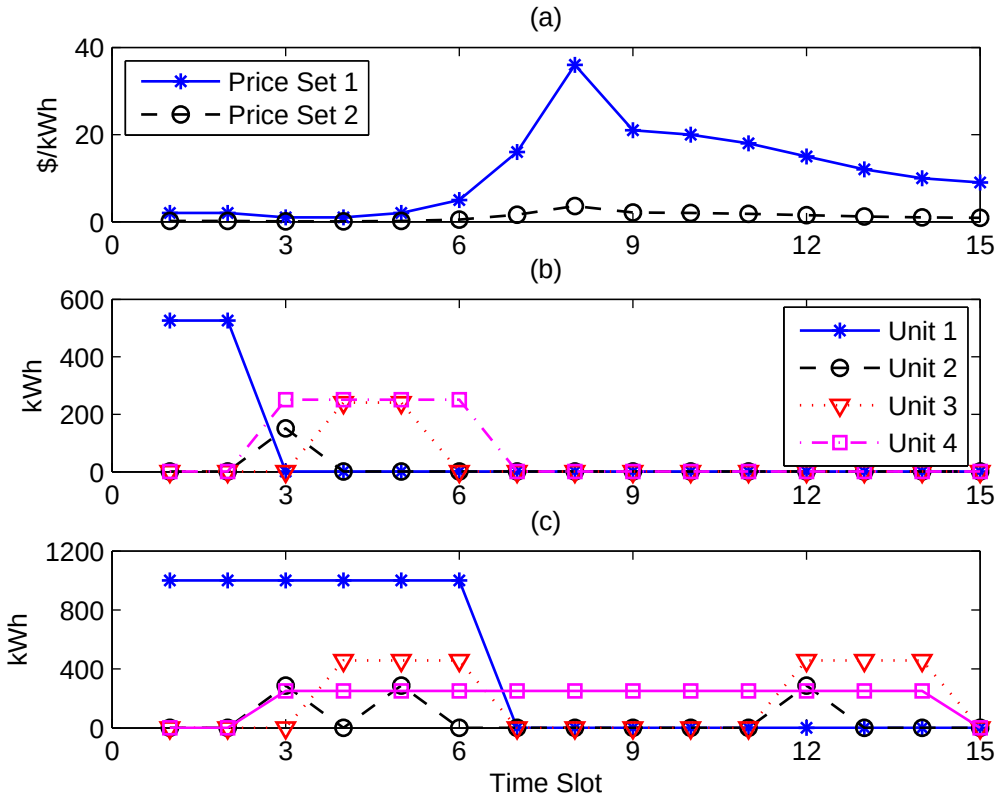

Figure 5.2: The data and results for load control in the illustrative example in Section 5.3.1: (a) two price sets, (b) the optimal operation of units under the first price set; (c) the optimal operation of units under the second price set.

Two sets of electricity price values are considered, as shown in Fig. 5.2(a). The optimal ILC solution corresponding to each set is obtained by solving optimization (7.4). For the first price set, the final products are produced at 48, 100, and 10.5 kg and the profit

is \$910. From Fig. 5.2(b), unit 2 operates only for one cycle at time slot 3 and consumes 151 kWh. Hence, based on (5.31), unit 2 operates at its minimum level 30 kg. This explains why unit 1 takes in 105 kg and unit 3 takes in 48 kg of input materials. Note that, although unit 3 could operate interruptably, it does not do so due to the lower price of electricity at time slot 5 compared to the later time slots. Finally, unit 4 starts operation as soon as its input materials are ready. It operates for two cycles at its maximum material level in time slots with lower electricity prices. Note that, the high price of final material m_8 when compared to its low production cost in cheap time slots, makes it worthy that unit 4 operates for more cycles than what is needed.

For the second price set, final products are produced at 274.3, 300, and 60 kg and the profit is \$24,756. As it can be seen in Fig. 5.2(c), unit 1 operates at its maximum level during cheaper time slots. Unit 2 takes into 57 kg of input materials since when unit 1 operates at its maximum level 200 kg, it produces 40 kg of m_4. Note that unit 3 employs its interruptibility and avoids expensive time slots in the second time slot of its second cycle. Unit 4 starts its operation as soon as its input materials are prepared and operates non-stop due to high profit in producing final material m_8.

It is worth pointing out that the availability of m_4 is a bottleneck in the production of final material m_6. This bottleneck can be reduced either by increasing the capacity of unit 1 or by increasing initial amount of m_4. For example, if capacity of unit 1 is increased to 400 kg, the amount of final products produced would be 365.7, 300, and 80 kg and the profit would increase to \$25,641. On the other hand, if initial amount of m_4 is increased to 100 kg, the amount of final products produced would be 400, 300, and 37.5 kg and the

profit would increase to $30,476.

Now impact of battery capacity on the profit is studied. As can be seen in Fig. 5.3, as battery capacity increases, profit also increases. However, increasing battery capacity after a certain point has no impact on profit.

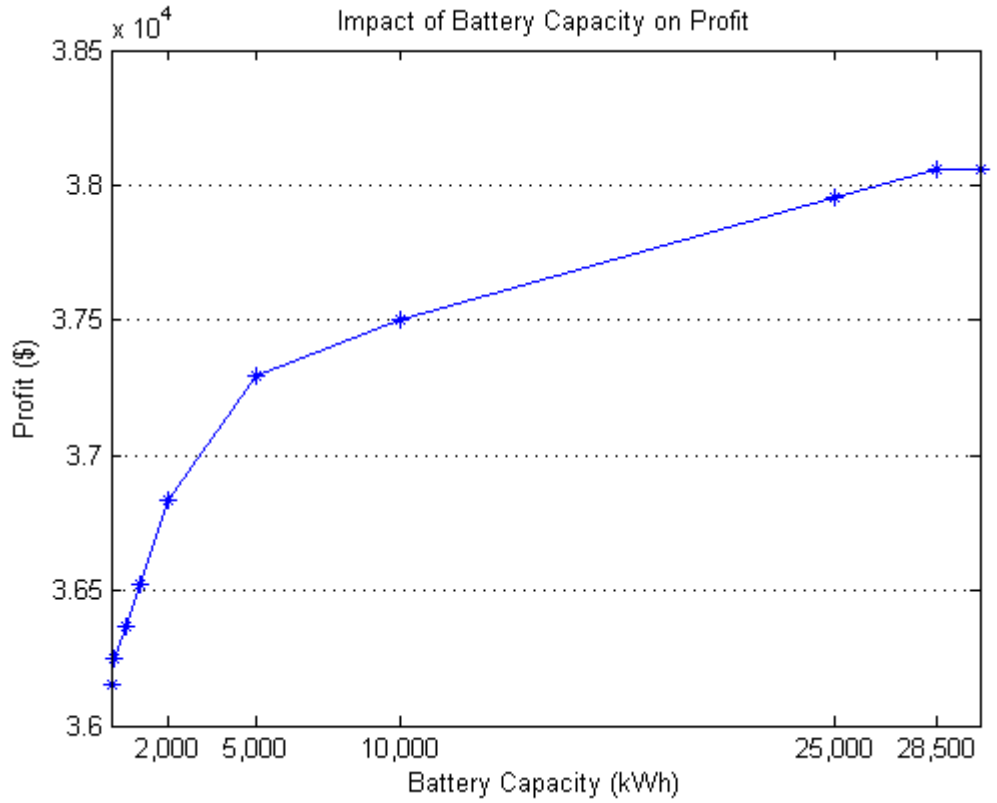

Figure 5.3: Impact of battery capacity on profit.

5.3.2 Steel Industry

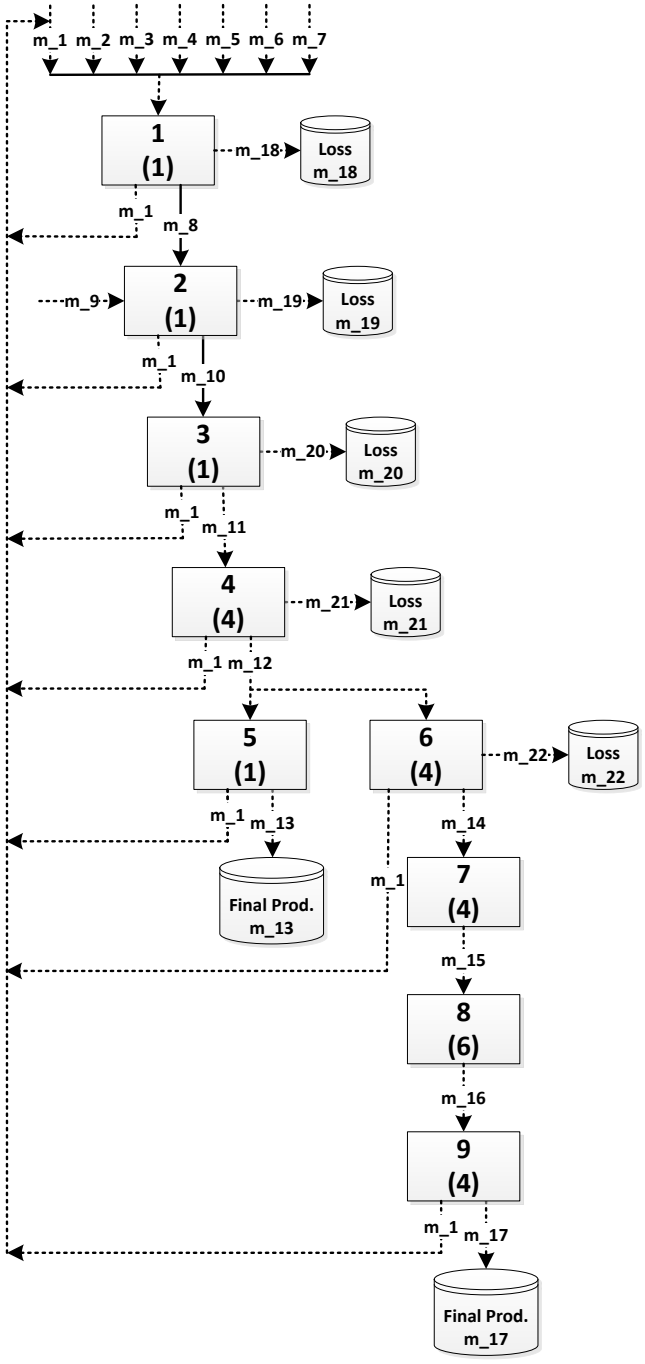

Figure 5.4: The flow diagram and interacting units for a steel mill industry.

Steel industry is energy intensive, and electricity cost accounts for a big portion of the total operational cost [39]. Fig. 5.4 shows flow diagram of a steel mill [40, 41]. Name of units and materials are given in Table 5.2. The numbers inside parenthesis in Fig. 5.4 represents batch cycle duration of each unit. Proportionality of input materials of unit 1 are 0.125, 0.376, 0.442, 0.036, 0.005, 0.014, and 0.002, and proportionality of input materials of unit 2 are 0.9996 and 0.0004, respectively [40]. Storage capacity for all materials is 20,000 tonne, except for material 8 and 10 which are zero. The initial amount is zero for all non-raw materials, 10,000 tonne for material 1, and 20,000 tonne for every other raw material. There is no cost to store materials. Unit price of initial materials is 0, 127.84, 163.54, 3.96, 5.85, 9.1, 11.6, and 10 \$/tonne, respectively. Unit price of final products is 710, 750, and 0 \$/tonne, respectively [42–44]. Daily background load in GJ is 0.06 for hours 1 and 21 to 24, 0.05 for hours 2 to 6, 0.09 for hours 7 and 10 to 12, 0.1 for hours 8 and 9, 0.08 for hours 13 to 18, and 0.07 for hours 19 and 20. Capacity, initial charge level, maximum charge rate, and maximum discharge rate of the battery system are 5000 kWh, 1500 kWh, 2500 kWh/hour, and 2500 kWh/hour (i.e., c-rate of 0.5), respectively. The load control horizon is $T = 48$ time slots (hours) and L_{max} is 5×10^5 kWh. The minimum needed final products are 20, 40, and 0 tonne, respectively.

The electricity price data for DAP is from PJM, starting March 20, 2014 [45]. To make different pricing methods comparable, we used DAP as reference and set the parameters for other pricing methods accordingly. Solar data is from [46], which includes one sunny day followed by a cloudy day. For the *no load control* case, problem (7.4) is solved for some flat electricity prices, which are calculated as follows: in DAP and CPP,

Table 5.2: Name of units and materials in Fig. 5.4.

Units	Materials	
1: Arc Furnace	m_1: Home Scrap	m_{10}: Treated Steel
2: Ladle Furnace	m_2: Purchased Scrap	m_{11}: Cast Steel
3: Slab Caster	m_3: DRI	m_{12}: Hot Band
4: Hot Strip Mill	m_4: Lime	m_{13}: Hot Band (F)
5: Skin Pass Mill	m_5: Alloys	m_{14}: Pickled Band
6: Pickle Line	m_6: Refractory	m_{15}: Cold Rolled
7: Cold Mill	m_7: Electrode	m_{16}: Annealed Band
8: Annealing Line	m_8: Liquid Steel	m_{17}: Cold Rolled (F)
9: Finishing Mill	m_9: Carbon	$m_{18} - m_{22}$: Losses

the average of DAP price; in ToUP, the average of off-peak and on-peak prices; in IBR, the average of base-load and high-load prices; and in PP, the average of regular price.

Impact of Pricing on Load Profile

The load profiles for different pricing models are shown in Fig. 5.5. We can see that the choice of pricing mechanism can significantly affect the optimal demand response of the steel industry. Note that while DAP is considered in [1], ToUP in [27–29], and CPP in [17], a wide range of smart pricing models are considered here, including PP and IBR which are not considered in other ILC literature.

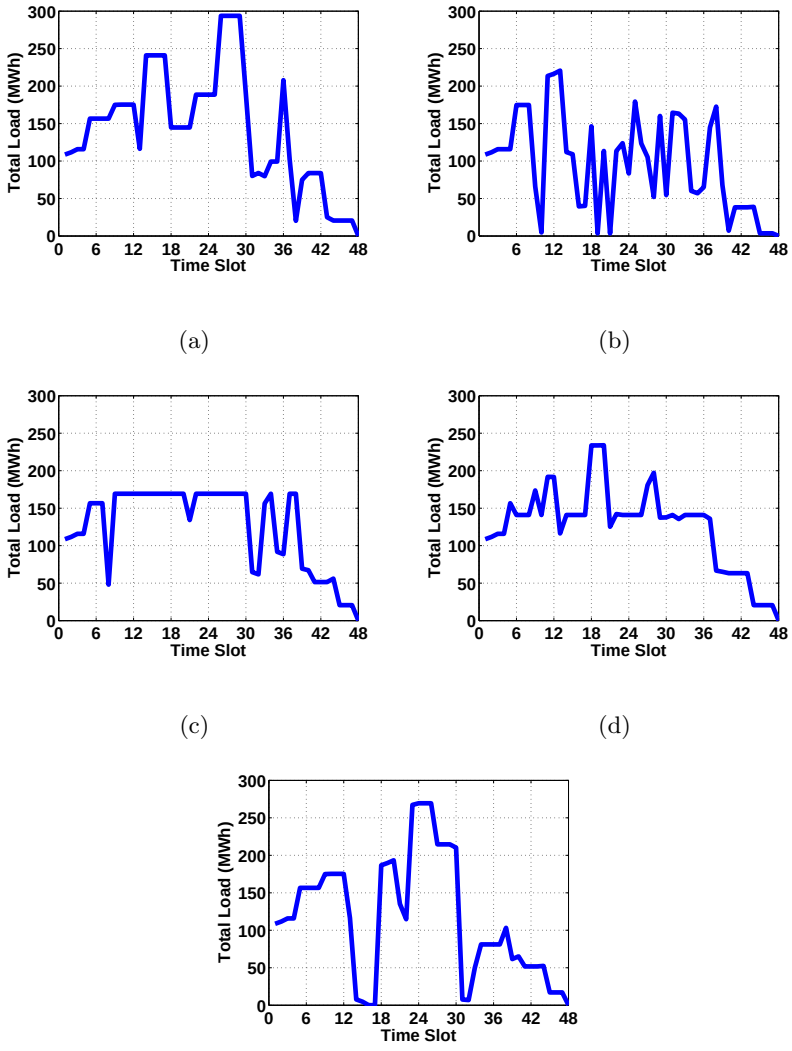

Figure 5.5: Optimal load profile: (a) DAP; (b) ToUP; (c) PP; (d) IBR; (e) CPP.

Advantages of Optimal Load Control

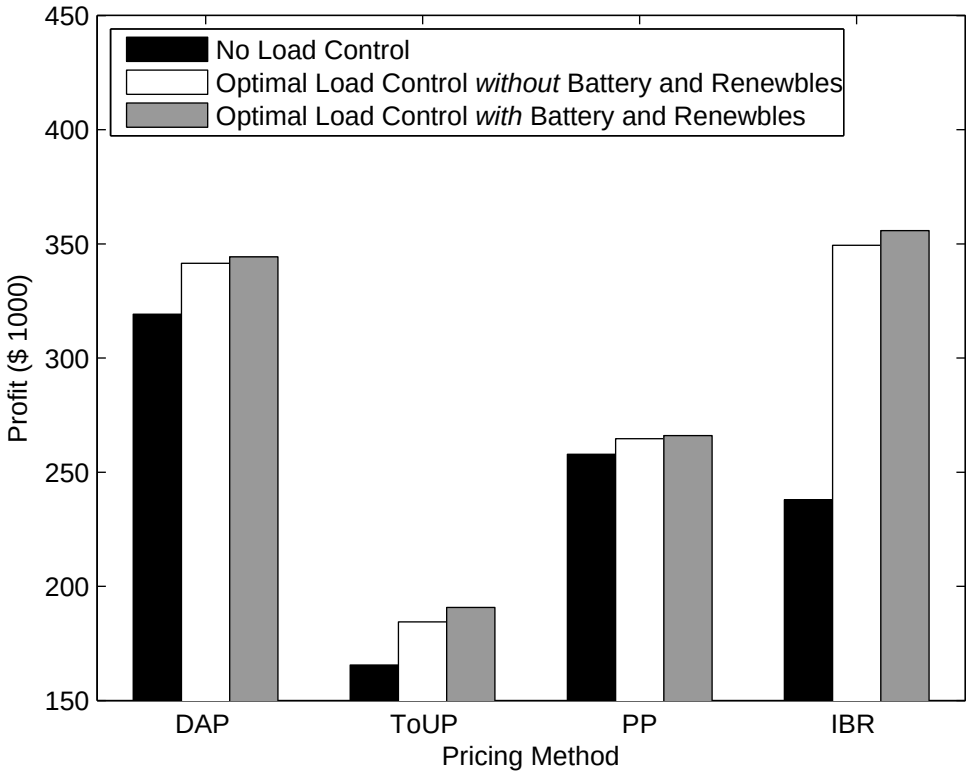

Figure 5.6: Profit under different price and resource scenarios.

From Fig. 5.6, in each pricing model, optimal scheduling results in higher profit. The improvement is 45% in presence of IBR and 10% in presence of ToUP. Furthermore, the use of behind-the-meter battery and renewable generator can further increase profit. However, since the total electricity usage of the units is much larger than the available renewable energy and the battery size, the profit improvement is small compared to the case with no battery and renewable energy. From Fig. 5.7, the battery is charged at low-price time slots and discharged at high-price time slots.

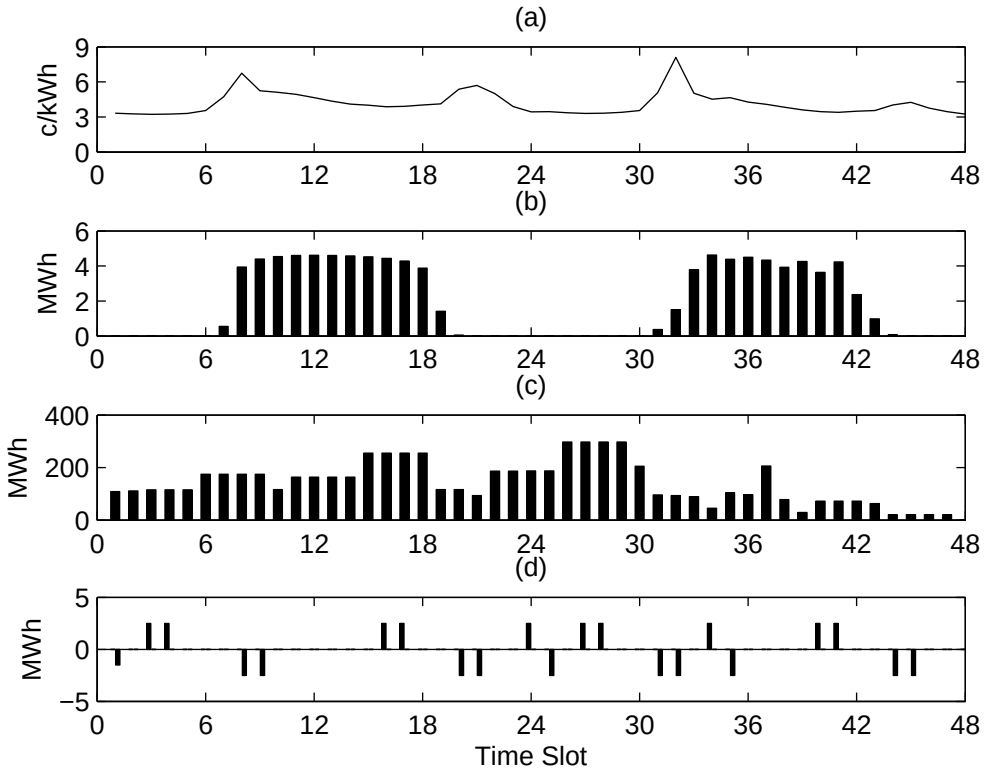

Figure 5.7: Operation with battery and renewable generator: (a) the retail price of electricity, (b) solar generation, (c) controllable load, (d) battery schedule.

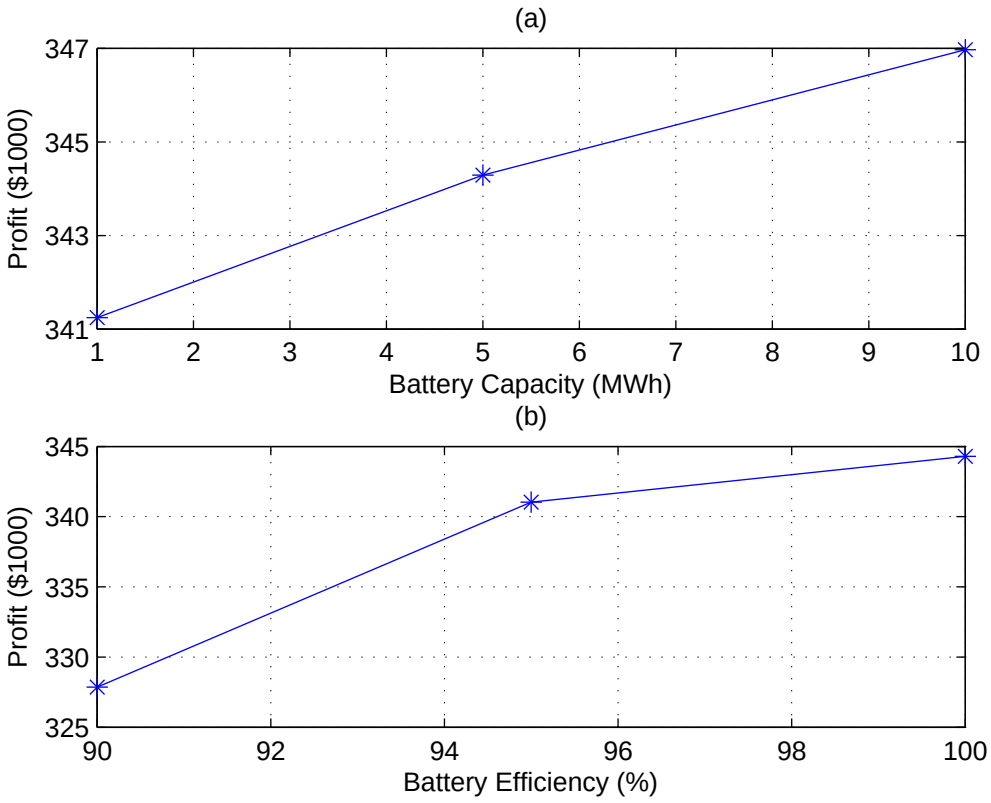

Figure 5.8: The impact of battery parameters on profit: (a) capacity, (b) efficiency.

Figs. 5.8(a) and (b) show the impact of battery capacity and battery efficiency on profit, respectively. We can see that profit increases as the battery capacity or battery efficiency increase.

Longer Scheduling Horizons

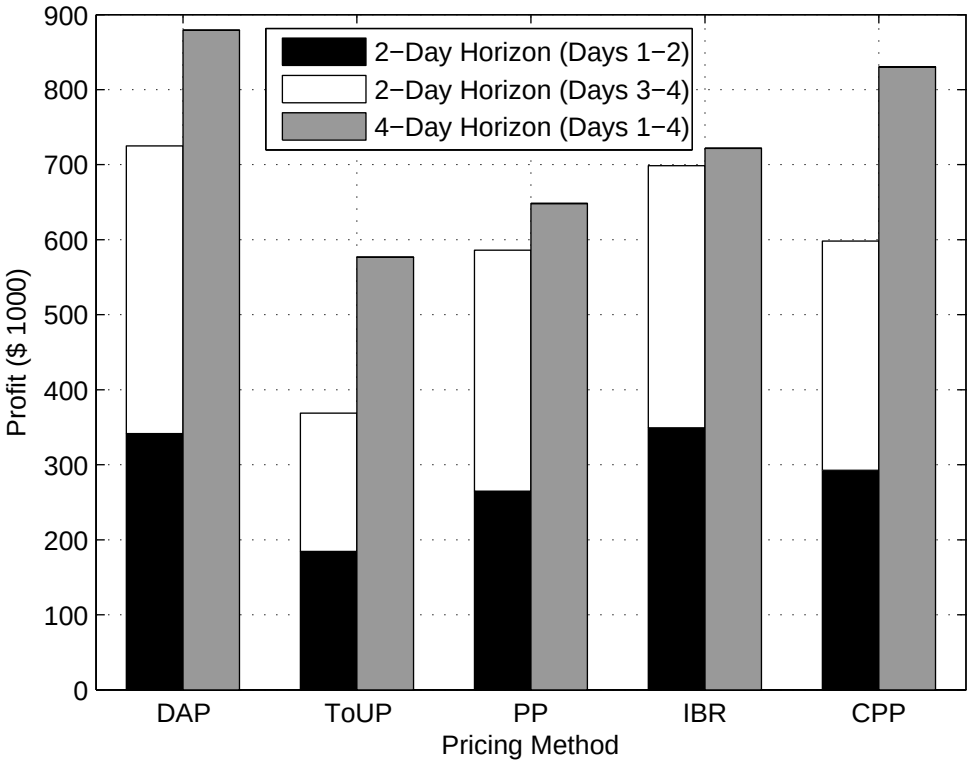

Figure 5.9: Impact of longer scheduling horizons on the overall profit.

From Fig. 5.9, profit increases as the scheduling horizon increases due to more time flexibility. The improvement in ToUP is over 50%, in CPP is around 40%, in DAP is over 20%, and in PP is over 10%.

Timing of CPP Warning

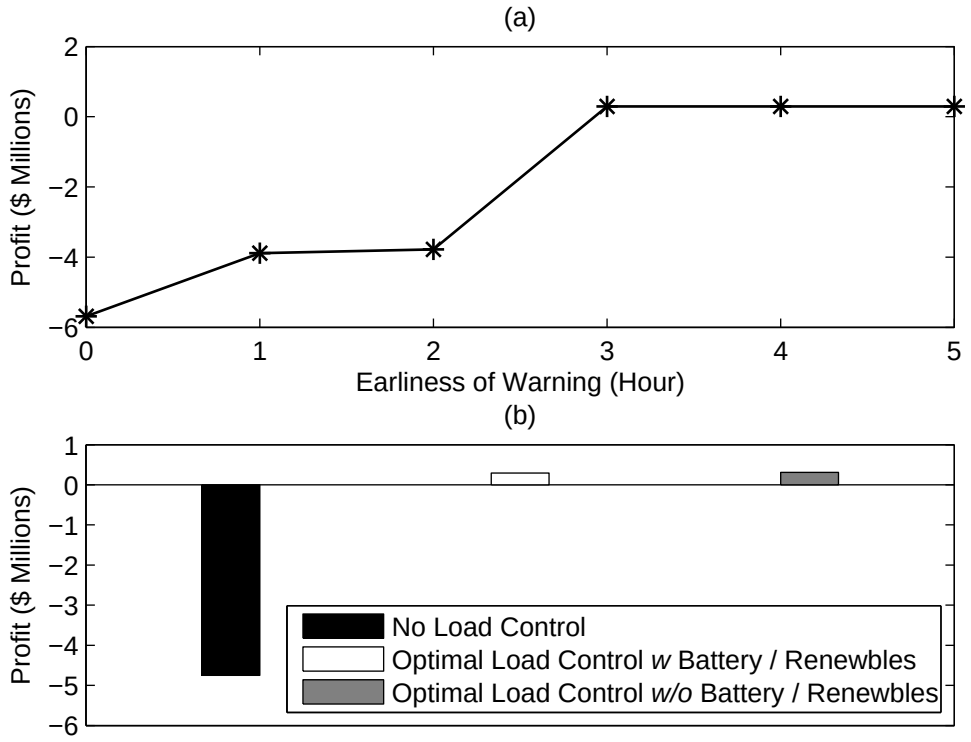

Figure 5.10: Results under CPP pricing method: (a) profit versus the earliness of warning; (b) profit under different control and resource scenarios.

From Fig. 5.10, late CPP warning can be very costly for industrial load since they often do not have enough flexibility to change the operation of their units in short notice, e.g., due uninterruptible nature of many units.

Optimization Time

Since ILC problem is an MIP problem, no formula for the complexity of the optimization can be given. One can reduce optimization time by choosing smaller gap tolerance

as explained in section 2.3. However, this may result in that result be further away from optimal solution. Therefore, we have a trade-off between optimization time and optimality of the solution. Fig. 5.11 shows the optimization time vs. relative gap tolerance for DAP in the steel industry case study with scheduling horizon of 48 hours. Based on Fig. 5.11, 3% relative gap tolerance seems a good choice since it is the smallest tolerance with an acceptable optimization time. However, this cannot be generalized to other problems.

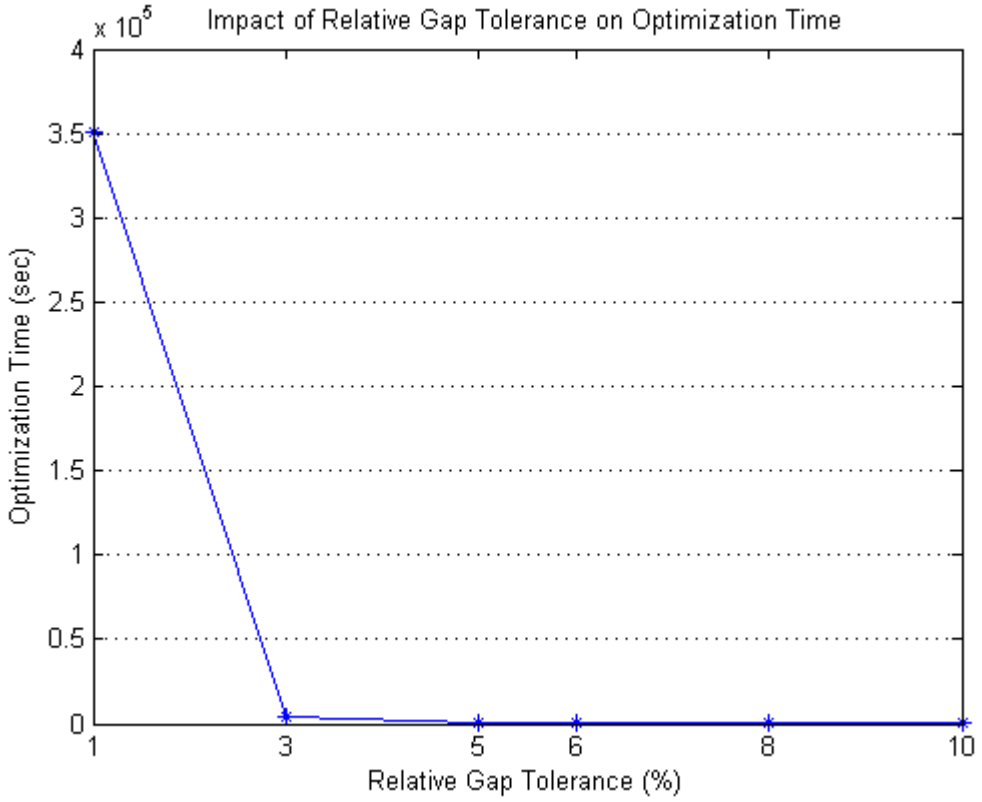

Figure 5.11: Impact of relative gap tolerance on optimization time.

5.4 Remarks

More constraints can be added to the formulation of optimal industrial load control, if needed.

5.4.1 Subunits

In this subsection, idea of decomposition of an industrial unit to virtual subunits is explained. Decomposition of an industrial unit to virtual subunits might be needed for one of the following reasons:

- power demand of the unit is variable during a cycle.
- not all input materials of the unit are injected at the beginning of a cycle (i.e., some are injected during a cycle).
- not all output materials of the unit are produced at the end of a cycle (i.e., some are produced during a cycle).

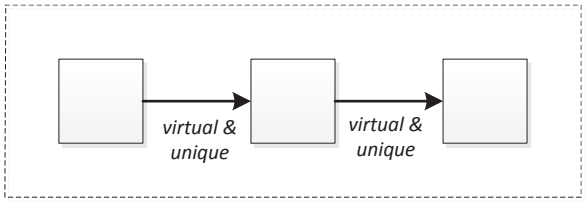

(a) Decomposition of an uninterruptible unit.

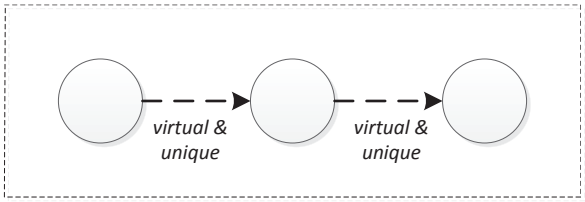

(b) Decomposition of an interruptible unit.

Figure 5.12: Decomposition of an industrial unit into three subunits.

Decomposition of an industrial unit depends on if the unit is uninterruptible or interruptible as shown in Fig. 5.12. As it can be seen, an uniterruptible unit is decomposed into a series of *uninterruptible* subunits with virtual and unique *immediate-consumed* materials. On the other hand, an interruptible unit is decomposed into a series of *interruptible* subunits with virtual and unique *non-immediate-consumed* materials. Note that materials are *virtual* in a sense that they are introduced for formulation purpose only and they are *unique* in a sense that they are not introduced in any other place of the system.

In addition to the structure shown in Fig. 5.12, the following constraints that are specific to subunits should also be considered:

1. At most one of the subunits should operate at a given time.

2. A virtual material produced by a subunit should be consumed *completely* by the next subunit (at the same cycle of the unit).

3. A preceding subunit cannot start a new cycle until all later subunits finish their cycle.

Let's formalize the above three constraints. For the sake of argument let's consider an example. Let's assume unit 1 should be decomposed into three subunits, 1a, 1b, and 1c as shown in Fig. 5.13 where the unit can be uniterruptible or interruptible.

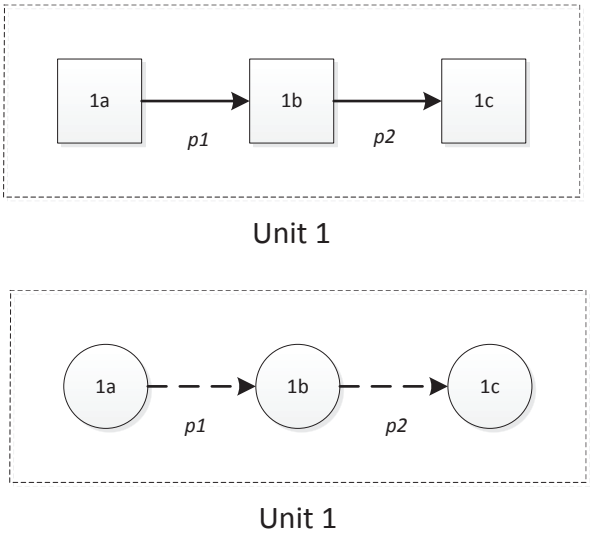

Figure 5.13: Unit 1 is decomposed into three subunits, 1a, 1b, and 1c. Materials $p1$ and $p2$ are virtual and unique materials.

At Most One Subunit Should Operate At a Given Time

$$x_{1a}[t] + x_{1b}[t] + x_{1c}[t] \leq 1, \quad \forall t \tag{5.44}$$

Complete Consumption of Virtual Materials

Let's consider virtual material $p1$ (similar equations can also be used for virtual material $p2$). We want "amount of virtual material $p1$ produced by subunit 1a=amount of virtual material $p1$ consumed by subunit 1b", i.e.,

$$\text{if } s_{1b}[t] - s_{1b}[t-1] = 1, \text{ then } \sum_{j=1}^{t} u_{1b}[j] = \sum_{j=1}^{t} y_{1a}[j]$$
$$\text{if } s_{1b}[t] - s_{1b}[t-1] = 0, \text{ then } \sum_{j=1}^{t} y_{1a}[j] \geq \sum_{j=1}^{t} u_{1b}[j]$$

The following captures that:

$$0 \leq \sum_{j=1}^{t} y_{1a}[j] - \sum_{j=1}^{t} u_{1b}[j] \leq \Omega * (1 - (s_{1b}[t] - s_{1b}[t-1])), \quad \forall t, \tag{5.45}$$

where Ω is a large enough number.

Number of Cycles of Subunits

$$\begin{aligned} 0 \leq s_{1a}[t] - e_{1b}[t] \leq 1, \quad \forall t, \\ 0 \leq s_{1b}[t] - e_{1c}[t] \leq 1, \quad \forall t, \\ 0 \leq s_{1a}[t] - e_{1c}[t] \leq 1, \quad \forall t. \end{aligned} \tag{5.46}$$

Notes

Note 1: In addition, the following changes should also be applied to electricity consumption parameters of subunits so that when unit i is not processing (i.e., neither of subunits $i,1$, $i,2$, and $i,3$ are operating), electricity consumption of the unit be standby electricity consumption $l_i^{\min}$.

Let $l_i^{\min}$ denote the true standby power of the original unit i. Make the following changes in the parameters:

$$\begin{aligned} l_{i,j}^{\min} &\leftarrow l_i^{\min}/3, \quad \forall j = 1,2,3, \\ d_{i,j} &\leftarrow d_{i,j} - 2 * l_i^{\min}/3, \quad \forall j = 1,2,3. \end{aligned} \tag{5.47}$$

Let's see why this works. When the unit is not processing, its total power consumption becomes:

$$l_{i,1}^{\min} + l_{i,2}^{\min} + l_{i,3}^{\min} = 3 * l_i^{\min}/3 = l_i^{\min}.$$

Also, when one of the sub-units (say subunit 2) is processing, we have:

$$c_{i,2} * M_i[t] + (d_{i,1b} - 2 * l_i^{\min}/3) + l_{i,1}^{\min} + l_{i,3}^{\min} = c_{i,2} * M_i[t] + d_{i,2}$$

Note 2: If an uninterruptible unit is decomposed, constraint (5.44) is the only constraint that really matters and the other constraints will be satisfied automatically.[1]

Note 3: Storage of virtual materials are virtual. Hence, initial amount of any virtual material available in storage should be *zero*.

5.4.2 Maintenance

Lets say interruptible unit i should be turned off for d_i time slot for maintenance, also known as down time. Then

$$x_i[t] = x_i[t+1] = ... = x_i[t+d_i-1] = 0 \tag{5.48}$$

[1] i.e., constraint (5.44) is necessary and sufficient condition for decomposition of an uninterruptible unit; constraint (5.45) will be satisfied since the virtual material is *immediate-consumed*. Constraint (5.46) will also be satisfied since for example subunit 1b will start its operation immediately after subunit 1a and based on constraint (5.44) only one of the subunits can operate at a given time and hence subunit 1a cannot start a new cycle when subunit 1b is operating.

Part III

Optimal Tuning in Full-Duplex Radios

Chapter 6

Introduction and Related Work

The wireless communication devices currently employed are all half-duplex and use either a frequency-division or time-division approach to transmit and receive. A more spectrally efficient approach, *full-duplex*, has received growing interest in the research community in the recent years. The main challenge in full-duplex is that the transmitted signal created by the device's own transmitter, known as *self-interference*, is very strong at the device's own receiver. Only by canceling self-interference to the noise floor, could full-duplex be realizable and the throughput be doubled.

As shown in [47], the methods for self-interference cancellation (SIC) can be grouped as *all-analog* [3, 4, 48–52], *all-digital* [53] and *hybrid* [47, 54–57]. In an all-analog method, RF interference is canceled at RF frontend by using its RF interference source. In an all-digital method, interference is canceled only after the RF interference has been converted into baseband and digitized. A hybrid method may use either a baseband-controlled transmit beamforming method to cancel interference at the RF frontend of receivers [56] or

use the RF signals tapped from the output of RF power amplifiers to cancel the interference after down-conversion to a lower frequency [47].

In general, a combination of these methods is required to fully realize full-duplex, but an all-analog cancellation is necessary in most situations. This is because (1) an all-analog cancellation can leave no or little additional noise in the residual self-interference, and (2) its performance in principle is not limited by the transmitter noise or by the transmitter nonlinearity.

The feasibility of all-analog SIC has been studied in [3, 4, 48–52]. In [48], two transmit antennas with a half-wavelength spacing difference relative to a receiving antenna is used to create a null at the receiver. This approach works for the narrowband case only, requires three antennas, and is sensitive to the spacing between antennas. The work in [49] can transmit and receive simultaneously only on different adjacent channels and not on the same channel. The all-analog canceler proposed in [50], in addition to an adjustable attenuator uses an adjustable phase shifter for each tap too. However, adjusting the phase of a typical phase shifter is not easy, and its insertion loss is significantly coupled with its phase. A closed-loop all-analog canceler is proposed in [52] which requires the knowledge of delay spread of the environment and is not applicable for an arbitrary environment. The most successful result was shown in [51], which uses an analog filter with uniformly distributed RF attenuators. However, in [51] distribution of tap delays for an arbitrary environment is not provided clearly and there is lack of theoretical insight.

In [3, 4], we have proposed a novel architecture for all-analog cancellation called *clustered* architecture and compare its performance with the *uniform* architecture, used

in [51]. We evaluate the statistical limits of each architecture through simulation and investigate the impact of imperfections of attenuators on the performance of the canceler. Furthermore, unlike previous works, we consider a wide range of realizations of a random interference channel model. We show how the cancellation performance in each architecture varies with the changes in the number of taps, and the relative delay between two adjacent taps of the canceler; environmental path loss; and the number of control bits, and the phase of the attenuators. We also investigate the impact of random perturbations to the uniform architecture. Finally, we investigate the impact of multi-level cancellation in each architecture.

Chapter 7

Optimal Tuning in All-Analog Radio Self-Interference Cancellation

7.1 Cancellation Channel Model

In Fig. 7.1(a), structure of a general all-analog canceler is shown. The goal in an all-analog canceler is to mimic the interference channel so that the output signal of the all-analog canceler be well-matched to the self-interference signal and consequently the residual interference be as small as possible. The matching can be done either in the frequency domain or in the time domain. Similar to [50, 51], our approach is in the frequency domain and the goal is to match frequency response of all-analog canceler to frequency response of self-interference channel.

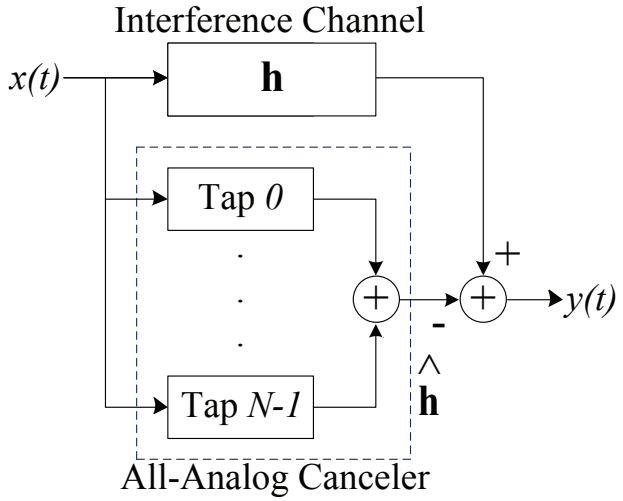

(a) System model for all-analog radio SIC

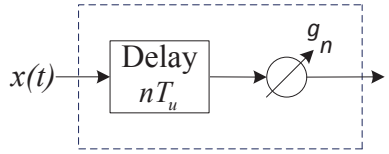

(b) nth tap of the uniform canceler,

$n = 0, 1, ..., N-1$

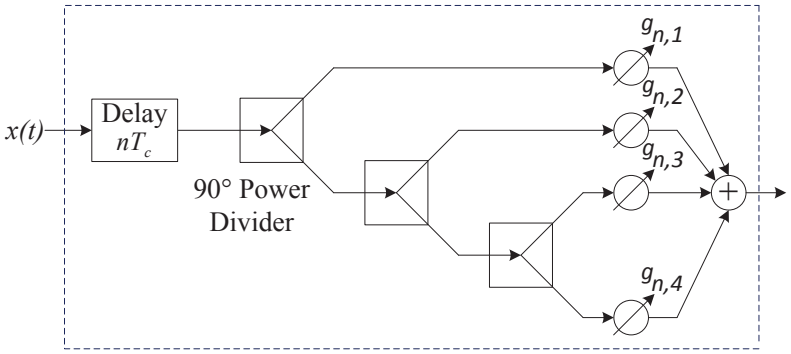

(c) nth c-tap of the clustered canceler, $n = 0, 1, ..., N-1$

Figure 7.1: (a) System model for all-analog radio SIC, (b) architecture of each tap of the uniform canceler, and (c) arcitecture of each tap of the clustered canceler. $x(t)$ is the transmitted signal and $y(t)$ is the residual interference.

The frequency response of a RF multipath interference channel $H(\omega)$ (before being converted to baseband) is

$$H(\omega) = \sum_{i=0}^{I-1} a_i e^{-j\omega\tau_i} \tag{7.1}$$

where $a_i > 0$ is the attenuatuin of the ith path, τ_i is the delay of the ith path, and I is the number of multipath components, where I, a_i, and τ_i are all unknown. The goal is to come up with a model that *approximates* the wireless multipath channel (7.1) well and is also easily *implementable* (particularly, no use of variable delays in the architecture).

One such a model is the uniform structure, used in [51]. The structure of each tap of the uniform canceler is shown in Fig. 7.1(b) where each tap consists of one adjustable attenuator and a fixed time delay. Therefore, based on Fig. 7.1(a) and 7.1(b), the frequency response of the uniform canceler is

$$\hat{H}_{\mathrm{u}}(\omega) = e^{-j\omega T_0} \sum_{n=0}^{N-1} g_n e^{-j\omega nT} \tag{7.2}$$

where T_0 is the delay of the zero-th tap (not shown in the figure), N is the number of taps, and T is the relative delay between two adjacent taps. Although the uniform canceler provides a good performance [51], it is sensitive to the carrier frequency, as will be shown later.

Here, we propose a clustered architecture where the RF attenuators are distributed in clusters. The structure of each tap of the clustered canceler, known as clustered-tap or *c-tap*, is shown in Fig. 7.1(c). Each c-tap is a cluster of four adjustable attenuators connected together via three cascaded 90° power dividers, and an RF cable for fixed time delay. A 90° power divider, splits an RF signal into two which differ from each other by 90° in phase.

Based on Fig. 7.1(a) and 7.1(c), frequency response of the clustered canceler is

$$\hat{H}_{\mathrm{c}}(\omega) = e^{-j\omega T_0} \sum_{n=0}^{N-1} [(g_{n,1} - g_{n,3}) + j(g_{n,2} - g_{n,4})] e^{-j\omega T n} \tag{7.3}$$

where N is the number of c-taps, T_0 is the delay of the zero-th c-tap, T is the relative delay between two adjacent c-taps, and $g_{n,i}$ is the gain of the ith attenuator in c-tap n.

Note that since $g_{n,i}$ represent an attenuation value, then we have $0 \leq g_{n,i} \leq 1$ for all $n = 0, 1, ..., N-1$ and $i = 1, 2, 3, 4$. Therefore, $(g_{n,1} - g_{n,3}) + j(g_{n,2} - g_{n,4})$ can produce any complex value with real and imaginary parts within $[-1, 1]$ interval. The intuition behind the clustered architecture is that each c-tap can match a large number of clustered multipaths in the interference channel. And if T is chosen small enough, $\hat{H}_{\mathrm{c}}(\omega)$ can be tuned to match a wide range of the interference channel, provided that the delay spread of the interference channel is no larger than NT.

The choice of T depends on the bandwidth of interest W. Particularly, $T = \frac{r_T}{W}$ where $r_T < 1$. Simulation results has shown that $r_T = 0.1$ is a good choice and the performance is not sensitive to r_T when it is around 0.1. Note that a fixed delay is desirable since building programmable delays is extremely hard. The choice of N depends on the desired performance and the delay spread of the interference channel T_d. Theoretically, we need $NT \geq T_d$ to have a perfect interference cancellation if all multipaths are significant. Note that in practice, T_d is not well defined and more importantly $NT \geq T_d$ could make N too large. Simulation results show that performance of clustere architecture for a wide range of interference channels having T_d much greater than NT, is good while T is chosen based on W only. Tuning algorithm for attenuators is discussed next.

7.2 Tuning Algorithm

7.2.1 Ideal Attenuators

Here, we assume attenuators are ideal, i.e., (1) they do not introduce any phase-shift and (2) they can provide any attenuation value between 0 and 1 precisely.

For SIC, we need to match the cancellation channel to the interference channel in the bandwidth of interest. Let $f_1, \cdots, f_K$ be K sample frequencies that uniformly span the interval $[f_c - \frac{W}{2}, f_c + \frac{W}{2}]$ where f_c is the carrier frequency. Let $\mathbf{h} = [H(\omega_1), H(\omega_2), \cdots, H(\omega_K)]^T$ where $\omega_k = 2\pi f_k$ for all $k = 1, ..., K$. Also Let $\hat{\mathbf{h}} = [\hat{H}(\omega_1), \hat{H}(\omega_2), \cdots, \hat{H}(\omega_K)]^T$ where $\hat{H}(\omega)$ represents either $\hat{H}_c(\omega)$ or $\hat{H}_u(\omega)$. Let in the clustered architecture, $\boldsymbol{g} = [g_{n,i}]$, $\forall n = 0, 1, ..., N-1$, $\forall i = 1, 2, 3, 4$, a $4N \times 1$ vector, and in the uniform architecture, $\boldsymbol{g} = [g_n]$, $\forall n = 0, 1, ..., N-1$, a $N \times 1$ vector. Then for each architecture we can write $\hat{\mathbf{h}} = \mathbf{T}\boldsymbol{g}$ where based on equation (7.3) or (7.2), the matrix $\mathbf{T}$ is easy to construct.

For the clustered architecture (and similarly for the uniform architecture), to determine the optimal $\boldsymbol{g}$, we solve the following optimization problem:

$$\min_{0 \le g_{n,i} \le 1, \forall n, \forall i} \left\| \begin{bmatrix} Re\{\mathbf{h}\} \\ Im\{\mathbf{h}\} \end{bmatrix} - \begin{bmatrix} Re\{\mathbf{T}\} \\ Im\{\mathbf{T}\} \end{bmatrix} \boldsymbol{g} \right\| \tag{7.4}$$

where Re and Im stand for real and imaginary parts. The above constrained problem is a *convex optimization* which can be solved by the CVX software [8]. Note that according to (7.3), solution to the optimization problem (7.4) is not unique.

7.2.2 Non-Ideal Attenuators

Here we assume attenuators are non-ideal. Particularly, two impairments introduced by attenuators are considered: phase-shift and quantization error. Let $g_{n,i} = r_{n,i}e^{j\theta_{n,i}}$ where $r_{n,i}$ and $\theta_{n,i}$ are the magnitude and phase-shift of attenuator $g_{n,i}$. In general, $\theta_{n,i}$ is a function of $r_{n,i}$, and to emphasize this fact, we rewrite $g_{n,i}$ as $g_{n,i} = r_{n,i}e^{j\theta_{n,i}(r_{n,i})}$.

Another impairment is quantization error introduced by digital-step attenuators. $r_{n,i}$ of each attenuator after quantization can only be such that $-20\log_{10} r_{n,i} \in \{0, \Delta, 2\Delta, ..., (2^{n_b}-1)\Delta\}$ where Δ is the step size and n_b is the number of control bits for the step attenuator. In other words, $r_{n,i}$ is quantized to $10^{-\frac{\Delta}{20}m_{n,i}}$ where $m_{n,i} = 0, 1, ..., 2^{n_b} - 1$. Therefore, $r_{n,i}e^{j\theta_{n,i}(r_{n,i})}$ is quantized to $10^{-\frac{\Delta}{20}m_{n,i}}e^{j\theta_{n,i}(m_{n,i})}$.

Here, for the clustered architecture, to determine optimal $\boldsymbol{g}$, we solve the following optimization problem:

$$\min_{m_{n,i}=0,1,...,2^{n_b}-1,\forall n,\forall i} \sum_k |H(\omega_k) - \hat{H}(\omega_k, \boldsymbol{m})|^2 \tag{7.5}$$

where $\boldsymbol{m} = [m_{n,i}]$, $\forall n, \forall i$ is a $4N \times 1$ vector. The optimization problem (7.5) is an *integer optimization* and it can be solved by relaxation of integer constraints on decision variables, i.e., replacing the constraint with $0 \leq m_{n,i} \leq 2^{n_b} - 1, \forall n, \forall i$, where $m_{n,i}$ is a real-valued variable. After solving the relaxed problem, each $m_{n,i}$ is rounded to the nearest integer. To solve the relaxed problem, the trust region reflective algorithm is used and the initial point for each $m_{n,i}$, is set to be $m_{\text{init}} = m_{\max} = 2^{n_b} - 1$. Note that at this point, attenuation of attenuators are at their maximum possible level and the magnitude of $\hat{H}(\omega_k, \boldsymbol{m})$ is at its lowest value, and as a result, the objective function has a high value.

Note that phase errors of non-ideal power dividers can be incorporated into phase-shift of attenuators. Also amplitude reduction of the transmitted signal due to power dividers will be captured by attenuators. Next, expressions for performance evaluation are defined.

7.3 Performance Evaluation

To evaluate performance of the all-analog canceler, we define a relative power of the residual interference for the rth realization of the interference channel and the mth frequency (in dB) as follows:

$$e^{(r)}(\omega_k) = 10\log_{10}\frac{\mid H^{(r)}(\omega_k) - \hat{H}^{(r)}(\omega_k) \mid^2}{\mid H^{(r)}(\omega_k) \mid^2} \tag{7.6}$$

Also we define three averaged residuals:

$$E_1^{(r)} = \frac{1}{K}\sum_{k=1}^{K} e^{(r)}(\omega_k) \tag{7.7}$$

$$E_2(\omega_k) = \frac{1}{N_r}\sum_{r=1}^{N_r} e^{(r)}(\omega_k) \tag{7.8}$$

$$E_3 = \frac{1}{KN_r}\sum_{r=1}^{N_r}\sum_{k=1}^{K} e^{(r)}(\omega_k) \tag{7.9}$$

where N_r is the number of realizations considered for the interference channel.

7.4 Simulation Results

In this section, the performance of the clustered and uniform architectures is compared through simulation. To have a fair comparison between two architectures, we choose

$N_u = 4N_c$ and $T_u = \frac{T_c}{4}$ where N_c and N_u are the number of taps, and T_c and T_u are the relative delay between two adjacent taps in the clustered and uniform architectures orderly. This would cause that two cancelers have the same number of attenuators $4N_c = N_u$, and also the same delay spread $N_u T_u = N_c T_c$.

Simulation results are based on the following values of parameters: $T_0 = 0$, $f_c = 2.4$ GHz, $W = 100$ MHz, $K = 1000$, $T_c = \frac{0.1}{W}$, $N_c = 4$, $N_u = 16$, $T_u = \frac{0.1}{4W}$. For non-ideal attenuators, we set $s = -0.0276$ rad/dB, $\Delta = 0.01$ dB, and $n_b = 13$ bits. Each simulation is based on $N_r = 100$ random interference channels.

7.4.1 Interference Channel Model

For statistical performance limits, the following random multipath interference channel model is used:

$$H(\omega) = \sum_{i=0}^{I-1} a_i e^{-j\omega\tau_i} \tag{7.10}$$

where I is the number of multipaths, τ_i is the delay of the ith multipath, and a_i is the amplitude of the ith multipath. To simulate a wide range of interference channels, it is assumed

$$a_i = \frac{\epsilon l_i d^\alpha}{(d + c\tau_i)^\alpha} \tag{7.11}$$

where l_i is a uniform random number within $(0, 1)$, $d = 0.03$m, $c = 3 \times 10^8$m/s, τ_i is a uniform random number within $(0, 1)\mu s$, and $\alpha \geq 1$ is the amplitude path loss exponent. We also choose $\tau_0 = 0$, $a_0 = \epsilon$, $I = 1000$ and $\epsilon = \frac{1}{1000}$. This choice of ϵ is to ensure that there is no effective gain in the interference channel since a canceler consisting of attenuators cannot provide a good cancellation in such a situation.

On the other hand, measurements of $H(\omega)$ is not perfect and the canceler uses noisy measurements $H_{noisy}(\omega)$ for tuning the attenuators rather than $H(\omega)$ where

$$H_{noisy}(\omega) = H(\omega) + w(\omega) \tag{7.12}$$

where $w(\omega)$ represents measurement noise. For each frequency, each of the real and imaginary parts of $w(\omega)$ is modeled as an independent uniform zero-mean random number. This noise results in an average SNR over the whole band $[f_c - \frac{W}{2}, f_c + \frac{W}{2}]$. In simulations, we set SNR=60dB.

7.4.2 Ideal Attenuators

Here, we investigate *limits* of the all-analog clustered and uniform cancelers. To do so, it is assumed perfect attenuators and no measurement noise ($w(\omega) = 0$). We also show that the performance of the clustered canceler is as good or better than the performance of the uniform canceler while the uniform canceler is also dependent to the choice of the carrier frequency.

Fig. 7.2 shows that performance of the uniform canceler is highly dependent to the choice of the carrier frequency and it can be completely ineffective if for a given T_u, f_c is not chosen properly (only 3dB cancellation). On the other hand, Fig. 7.4 shows the performance of the uniform canceler when a proper carrier frequency is chosen and the performance of the uniform canceler is at its best.

Fig. 7.3 shows that performance of the clustered canceler for $f_c = 2.4GHz$. Note that the clustered canceler is not dependent to the choice of the carrier frequency and the results for any other f_c would be the same (shown in Fig. 7.9).

Fig. 7.4(a) and 7.3(a) show that as the number of taps N increases, the residual interference decreases.

Fig. 7.4(b) and 7.3(b) show how the residual interference varies with frequency for different values of N. It can be seen that the residual interference is relatively high near the edges of the frequency band of interest.

Fig. 7.5 shows $r_T = 0.1$ is a good choice for $T = \frac{r_T}{W}$ and the performance is not sensitive to r_T when it is around 0.1. Also Fig. 7.5(b) shows that uniform canceler can be ineffective if for a given f_c, T_u is not chosen properly and $f_c T_u$ is equal to an integer. This is one of the advantages of the clustered canceler in compare to the uniform canceler.

Fig. 7.6 shows that performance is better in more obstructive environment (larger α). Fig. 7.6(a) shows that for the clustered canceler, the residual interference decreases linearly as the amplitude path loss exponent α increases.

Fig. 7.7 shows the impact of bandwidth of interest W on performance of the clustered architecture with ideal attenuators. It shows that the residual interference decreases as W decreases.

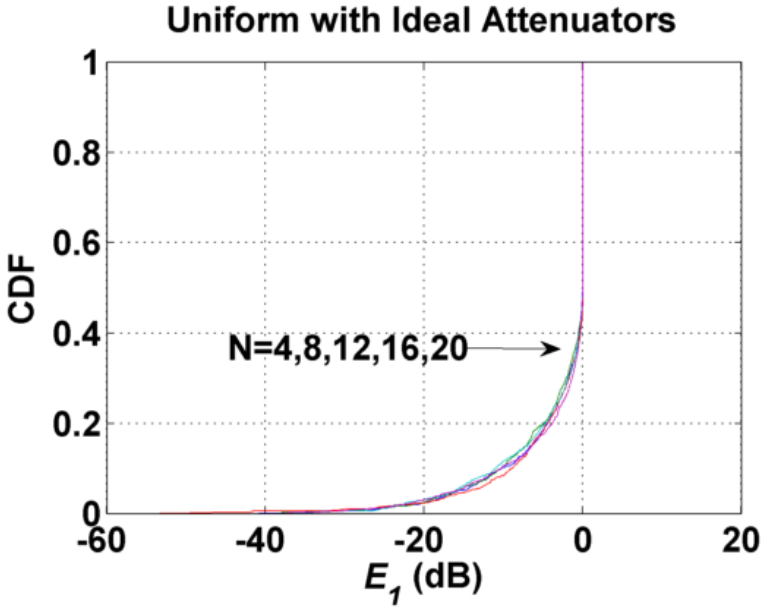

(a) CDF of E_1

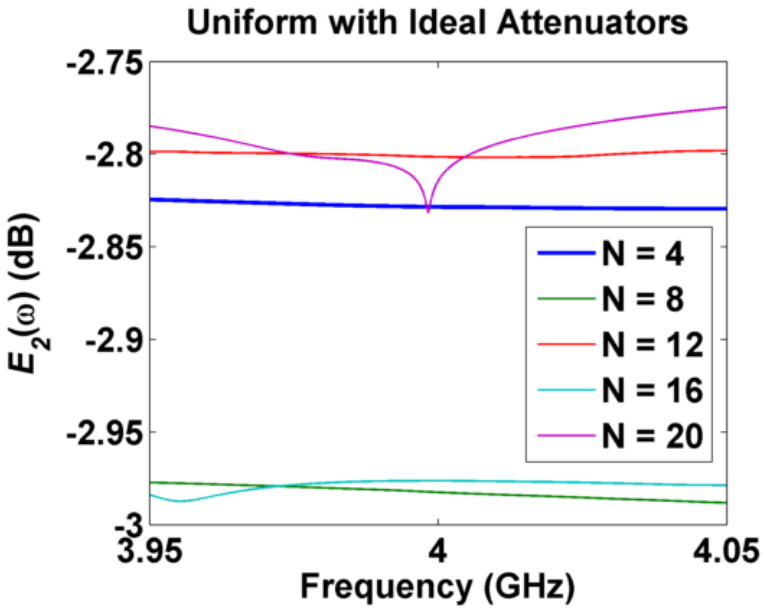

(b) $E_2(\omega)$ vs. frequency

Figure 7.2: Performance of uniform canceler with ideal attenuators and an improper f_c ($f_c = 4GHz$).

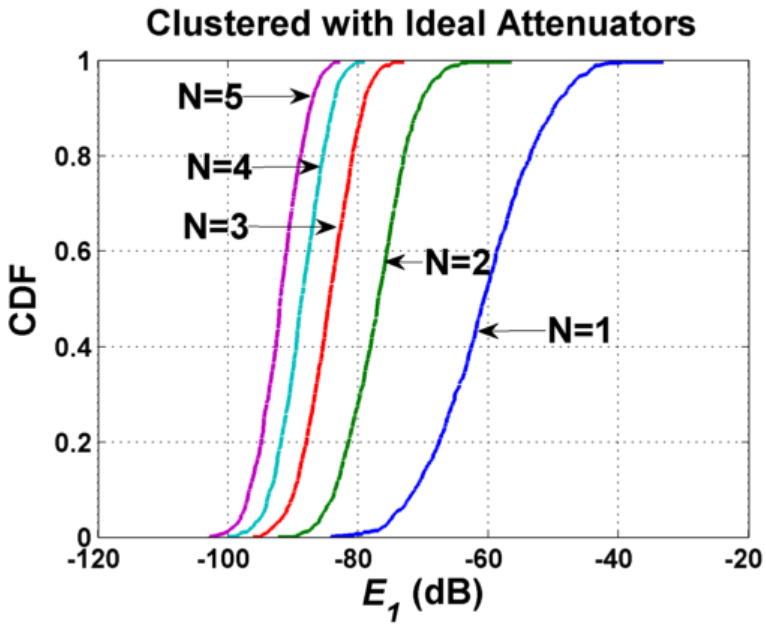

(a) CDF of E_1

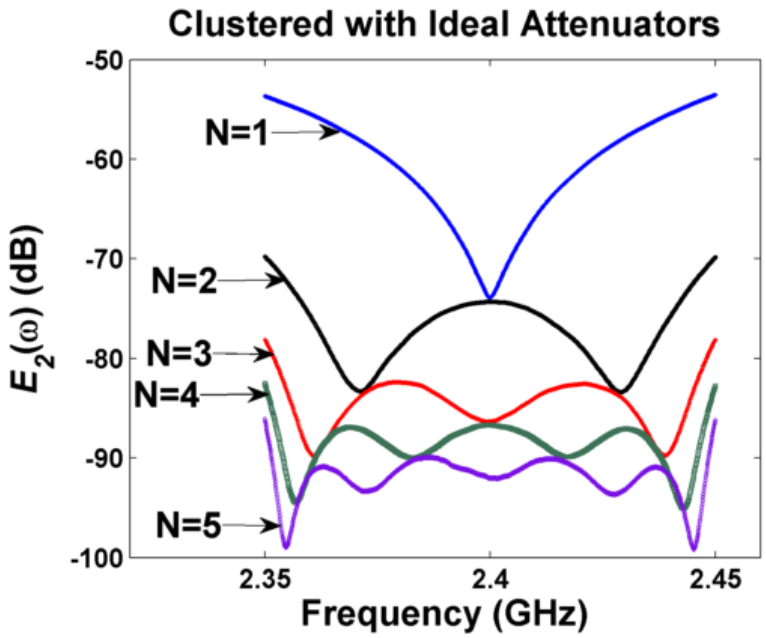

(b) $E_2(\omega)$ vs. frequency

Figure 7.3: Performance of a clustered canceler with ideal attenuators. $f_c = 2.4GHz$.

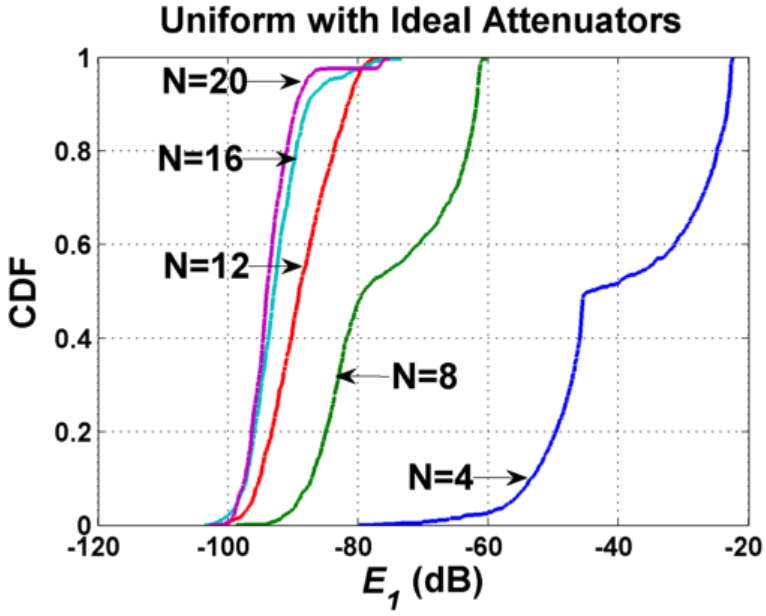

(a) CDF of E_1

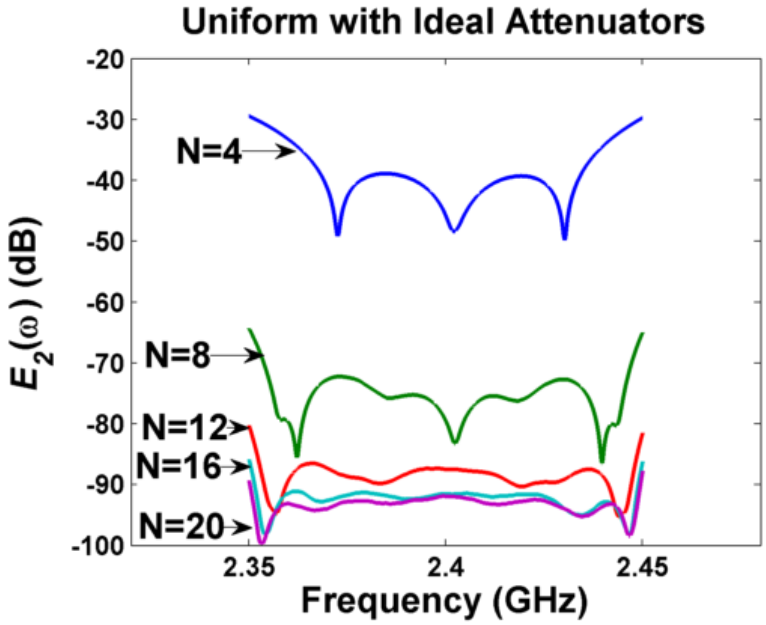

(b) $E_2(\omega)$ vs. frequency

Figure 7.4: Performance of a uniform canceler with ideal attenuators and a proper f_c ($f_c = 2.4GHz$).

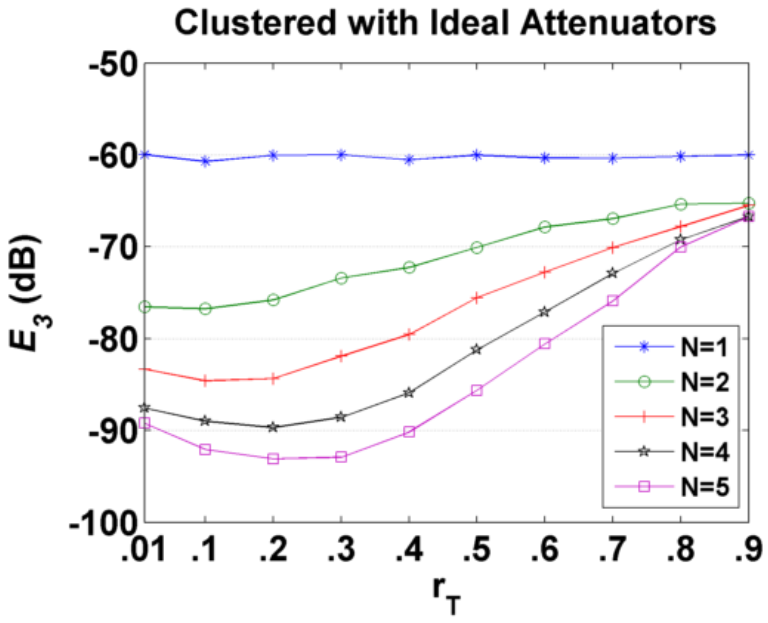

(a) Clustered Canceler

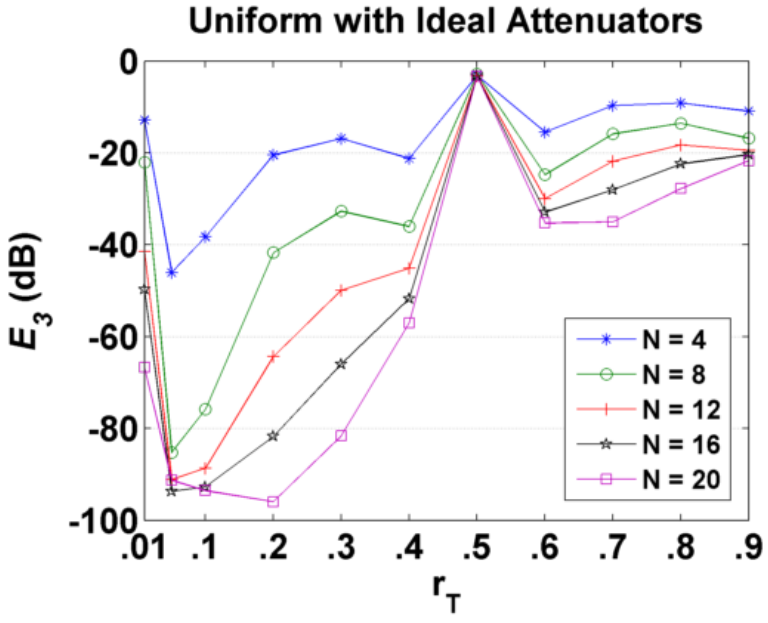

(b) Uniform Canceler

Figure 7.5: Impact of choice of $T_c = \frac{r_T}{W}$ and $T_u = \frac{r_T}{4W}$ on the performance of the cancelers with ideal attenuators for different values of N. $f_c = 2.4GHz$

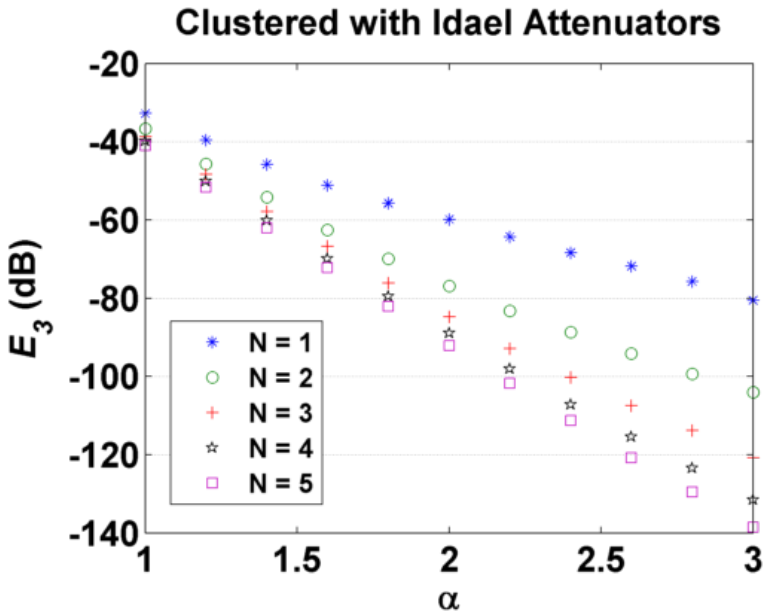

(a) Clustered Canceler

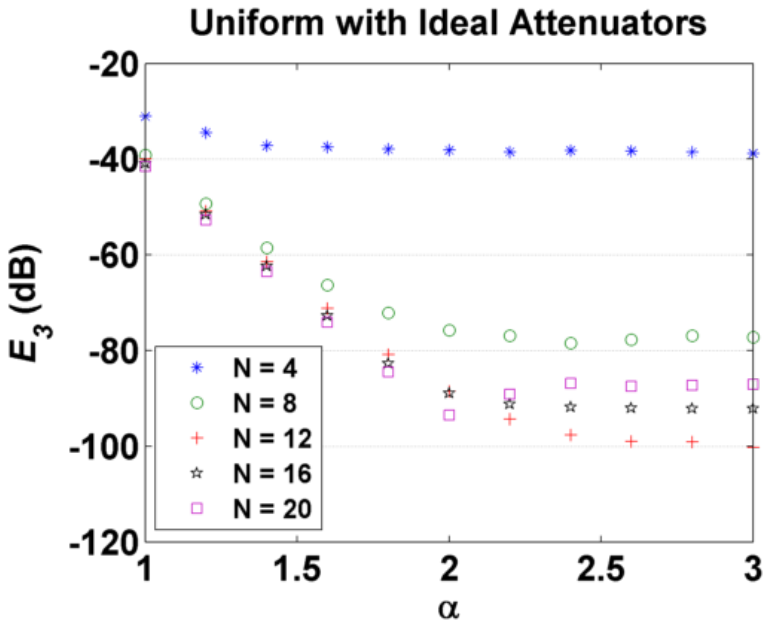

(b) Uniform Canceler

Figure 7.6: Impact of amplitude path loss exponent α on the performance of the cancelers with ideal attenuators for different values of N. $f_c = 2.4GHz$

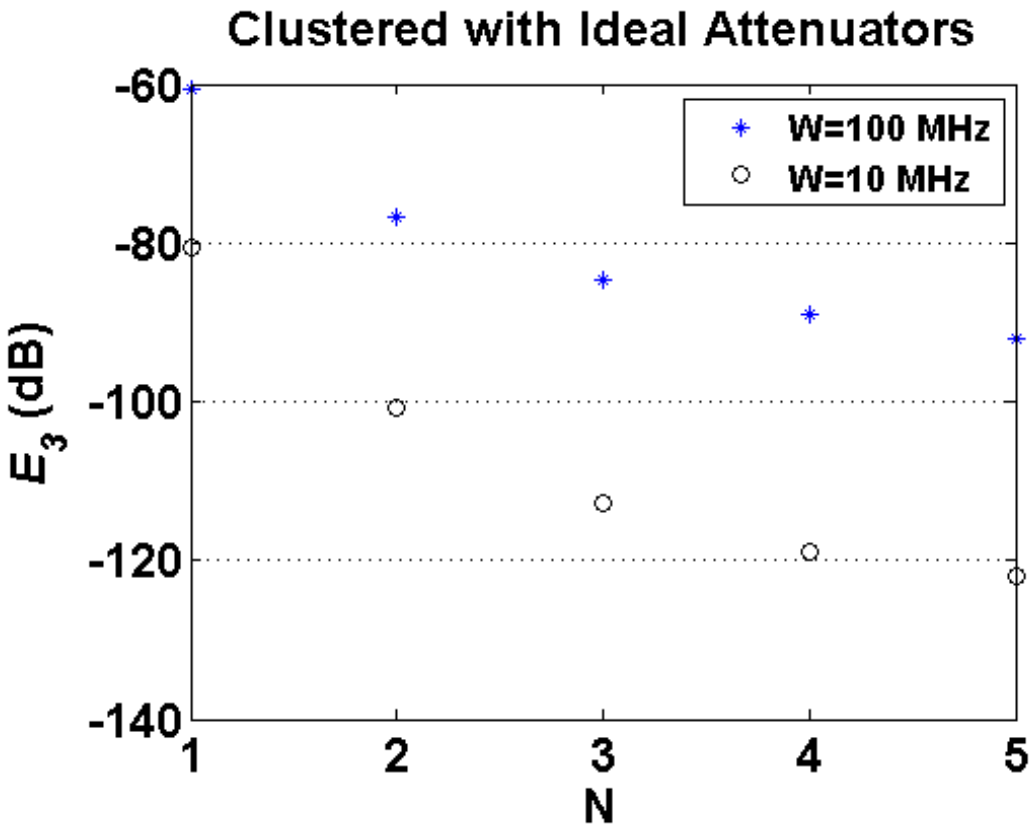

Figure 7.7: Impact of N and W on performance of the clustered canceler with ideal attenuators.

7.4.3 Non-Ideal Attenuators

As mentioned in Section 7.2.2, two impairments for non-ideal attenuators are considered, phase-shift and quantization error. Phase-shift introduced by an attenuator $\theta_{n,i}(r_{n,i})$ can be modeled as a linear function of attenuator magnitude $r_{n,i}$ in dB, i.e., $\theta_{n,i}(r_{n,i}) \propto -20\log_{10} r_{n,i}$ [52]. Therefore, $g_{n,i} = r_{n,i}e^{j\gamma \log_{10} r_{n,i}}$ where $\gamma_{n,i} = -20s_{n,i}$ and $s_{n,i}$ is the slope of phase (in radian) vs. attenuation (in dB). For simulation, it is assumed $s_{n,i} = s, \forall n, \forall i$, and consequently, $\gamma_{n,i} = \gamma$. As a result, frequency response of the clustered

canceler becomes

$$\hat{H}_c(\omega_k, \boldsymbol{r}) = \sum_{n=0}^{N-1} \left[\left(r_{n,1} e^{j\gamma \log r_{n,1}} - r_{n,3} e^{j\gamma \log r_{n,3}} \right) + j \left(r_{n,2} e^{j\gamma \log r_{n,2}} - r_{n,4} e^{j\gamma \log r_{n,4}} \right) \right] e^{-j\omega_k nT}$$

After quantization by digital-step attenuators, frequency response of the clustered canceler becomes

$$\hat{H}_c(\omega_k, \boldsymbol{m}) = \sum_{n=0}^{N-1} \left[(\eta^{m_{n,1}} - \eta^{m_{n,3}}) + j \, (\eta^{m_{n,2}} - \eta^{m_{n,4}}) \right] e^{-j\omega_k nT} \tag{7.13}$$

where $\eta = \left(10 e^{j\gamma}\right)^{-\frac{\Delta}{20}}$.

Note that the gradient of the objective function of the optimization problem (7.5) would be

$$\frac{\partial J(\boldsymbol{m})}{\partial \boldsymbol{m}} = \sum_k \left[\left(\hat{H}_c(\omega_k, \boldsymbol{m}) - H(\omega_k) \right) \cdot \frac{\partial \hat{H}_c^*(\omega_k, \boldsymbol{m})}{\partial \boldsymbol{m}} + \left(\hat{H}_c(\omega_k, \boldsymbol{m}) - H(\omega_k) \right)^* \cdot \frac{\partial \hat{H}_c(\omega_k, \boldsymbol{m})}{\partial \boldsymbol{m}} \right]$$

which can be rewritten as

$$\frac{\partial J(\boldsymbol{m})}{\partial \boldsymbol{m}} = 2 \sum_k \mathrm{Re} \left\{ \left(\hat{H}_c(\omega_k, \boldsymbol{m}) - H(\omega_k) \right)^* \cdot \frac{\partial \hat{H}_c(\omega_k, \boldsymbol{m})}{\partial \boldsymbol{m}} \right\}$$

where $\frac{\partial J(\boldsymbol{m})}{\partial \boldsymbol{m}}$ is a $1 \times 4N$ vector and $(1, 4n+i)^{th}$ element of $\frac{\partial \hat{H}_c(\omega_k, \boldsymbol{m})}{\partial \boldsymbol{m}}$ is:

$$\frac{\partial \hat{H}_c(\omega_k, \boldsymbol{m})}{\partial m_{n,i}} = c_i \cdot \eta^{m_{n,i}} \cdot \ln \eta \cdot e^{-j\omega_k nT}$$

and $c_i = 1, j, -1, -j$ for $i = 1, 2, 3, 4$ orderly. Gradient of the objective function then would be transpose of $\frac{\partial J(\boldsymbol{m})}{\partial \boldsymbol{m}}$. For uniform architecture, a similar analysis can be done to evaluate the gradient of the objective function.

Fig. 7.8 shows impact of the parameters of non-ideal attenuators on the performance of the cancelers. As shown in Fig. 7.8(a), as n_b increases, performance improves. However, the performance saturates when n_b is beyond a threshold for a given Δ (not

shown here). This threshold depends on the value of Δ since the maximum attenuation is $(2^{n_b} - 1)\Delta$dB.

Fig. 7.8(b) shows impact of phase-shift of attenuators. As it can be seen, phase-shift does not have much impact on the performance. Since phase-shift introduced by attenuators does not have much impact on the performance, one can ignore phase-shift and considers only quantization error of attenuators in the formulation in order to have a faster tuning algorithm.

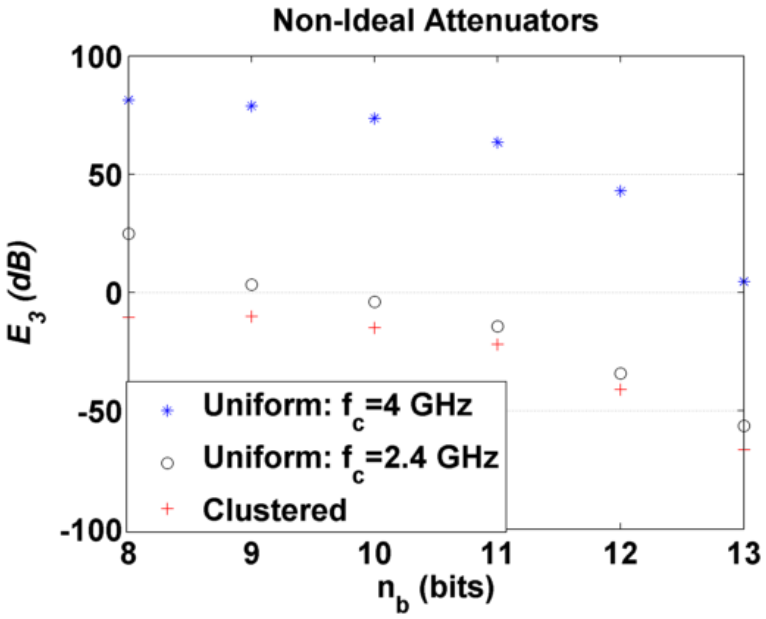

(a) Impact of n_b on performance. $N_c = 4, N_u = 16, \Delta = 0.01dB$.

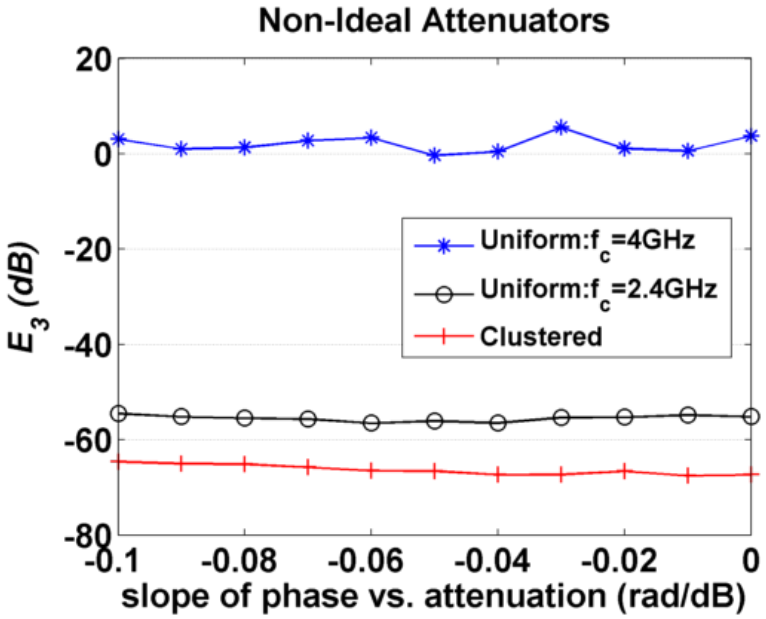

(b) Impact of phase-shift of attenuators on performance. $N_c = 4, N_u = 16, \Delta = 0.01dB, n_b = 13$.

Figure 7.8: Impact of n_b and phase-shift of attenuators on performance.

Ignoring Phase-Shift

Let $g_{n,i}$ represents optimal solution before quantization in non-dB and $\hat{g}_{n,i}$ represent value of $g_{n,i}$ after quantization. Then, we have $-20\log_{10}\hat{g}_{n,i} = m_{n,i}\Delta$ or $\hat{g}_{n,i} = 10^{-\frac{\Delta}{20}m_{n,i}}$ where $m_{n,i} = 0, 1, ..., 2^{n_b} - 1 = m_{\max}$. Consequently, we have $\hat{g}_{n,1} - \hat{g}_{n,3} = 10^{-\frac{\Delta}{20}m_{n,1}} - 10^{-\frac{\Delta}{20}m_{n,3}}$ and $\hat{g}_{n,2} - \hat{g}_{n,4} = 10^{-\frac{\Delta}{20}m_{n,2}} - 10^{-\frac{\Delta}{20}m_{n,4}}$. Then we want

$$\min_{m_{n,i}=0,1,...,2^{n_b}-1,\forall n,\text{for}i=1,3} |(g_{n,1} - g_{n,3}) - (10^{-\frac{\Delta}{20}m_{n,2}} - 10^{-\frac{\Delta}{20}m_{n,4}})| \tag{7.14}$$

and similar equation for $i = 2, 4$. Optimization (7.14) is a integer optimization problem. Note that the objective function is non-linear, non-quadratic, and non-convex. Two algorithms is considered to solve the optimization problem (7.14). One is exhaustive search. The other is a much more efficient algorithm explained here.

Algorithm: Consider one of the decision variables $m_{n,1}$ fixed and solve for the other decision variable $m_{n,3}$. Since $m_{n,3}$ may be non-integer, consider floor and ceil of $m_{n,3}$ instead. We do this for all values of $m_{n,1}$, i.e., $m_{n,1} = 0, 1, ..., m_{\max}$, and at each stage if we get a better result (lower objective function), we update the optimal solution.

The exhaustive search has complexity of $O(m_{\max}^2)$ while the suggested algorithm has complexity of $O(m_{\max})$ which is much more efficient than the exhaustive search.

7.4.4 Randomized Uniform

Here, we consider the case that the relative delay between two adjacent taps of the uniform structure, is not fixed. This may be due to imperfect length of cables used to implement time delays. Particularly, in tap n, instead of having delay of nT, there is delay

of $T_n = nT_u + \delta_n$, and as a result we have

$$\hat{H}_{\mathrm{r}}(\omega) = e^{-j\omega T_0} \sum_{n=0}^{N-1} g_n e^{-j\omega(nT_u+\delta_n)} \tag{7.15}$$

where $\delta_0 = 0$ and δ_n for $n = 1, ..., N-1$ are i.i.d. uniform random variables in $(-\delta_{max}, \delta_{max})$ and $\delta_{max} = T_u p$. For simulation, $p = 1\%, 2\%, 5\%, 10\%, 20\%$ is chosen.

Fig. 7.9 shows that in the uniform canceler for an improper carrier frequency, even changing T_u within 20% of T_u, does not improve the performance. It also shows that the clustered canceler is robust to the choice of the carrier frequency.

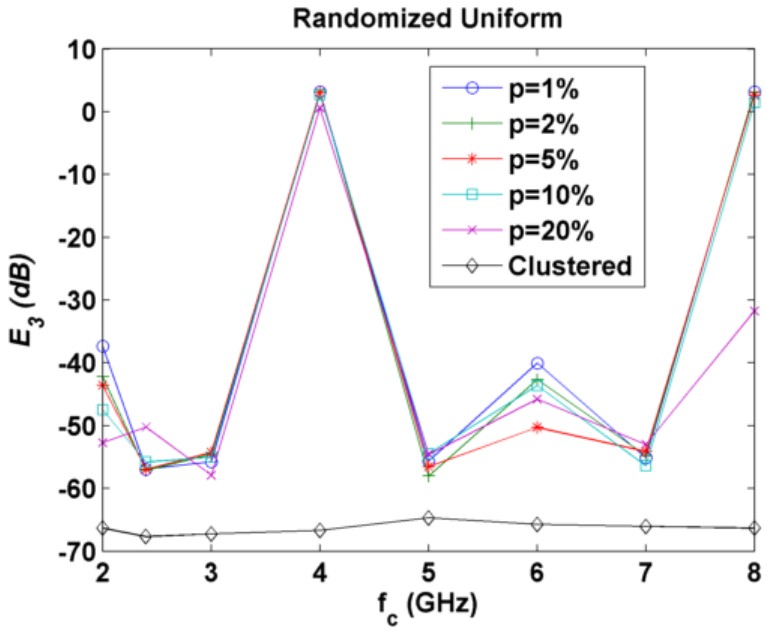

Figure 7.9: Impact of perturbation in T_u on performance.$N_u = 16, \Delta = 0.01dB, n_b = 13$.

7.4.5 Multi-Level Cancellation

Structure of a general two-level canceler is shown in Fig. 7.10 where the residual of the first-level canceler is further reduced by the second level. Let the number of taps and

relative delay between two adjacent taps in the first level be N_1 and T_1 and in the second level be N_2 and T_2. Here, we want to investigate if the multi-level canceler outperforms the single-level canceler where two cancelers have the same total number of taps and also the same delay spread. In other words, if the number of taps and the relative delay between two adjacent taps in the single-level canceler be N and T, such that $N = N_1 + N_2$ and $NT = \max\{N_1T_1, N_2T_2\}$, for a given interference channel which structure performs better. To evaluate the overall performance of multi-level canceler, the expression (7.6) is modified as follows:

$$e^{(r)}(\omega_k) = 10\log_{10}\frac{\mid H^{(r)}(\omega_k) - \hat{H}_1^{(r)}(\omega_k) - \hat{H}_2^{(r)}(\omega_k) \mid^2}{\mid H^{(r)}(\omega_k) \mid^2} \tag{7.16}$$

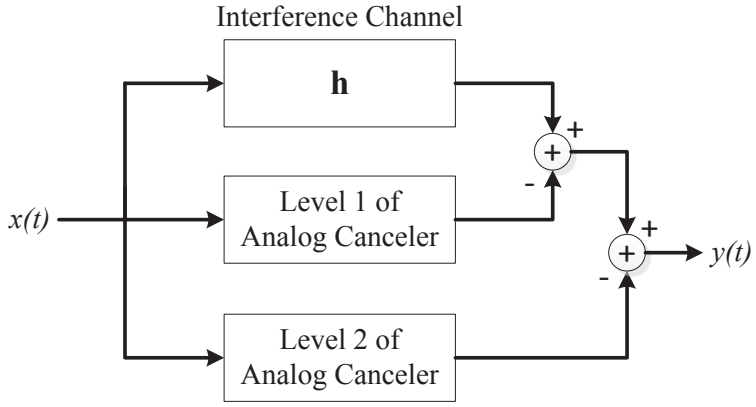

Figure 7.10: System model for two-level all-analog canceler.

First, impact of two-level canceler on the clustered architecture is simulated and compared to the single-level clustered canceler. For the single-level with $N = 4$ and $T = \frac{0.1}{W}$, there is 67 dB cancellation, i.e., $E_3 = -67$ dB. For two-level canceler for $N_1 = 1$, $N_2 = 3$, $T_1 = \frac{0.1}{W}$, and $T_2 = \frac{NT}{N_2}$, there is 61 dB cancellation for the first level but 77 dB for the

overall two-level cancellation. Interestingly, two-level clustered canceler outperforms the single-level clustered canceler.

Next, impact of two-level canceler on the uniform architecture is simulated and compared to the single-level uniform canceler. We assume a good carrier frequency for the uniform canceler ($f_c = 2.4GHz$). For the single-level with $N = 16$ and $T = \frac{0.1}{4W}$, there is 55 dB cancellation. For the two-level canceler for $N_1 = 4$, $N_2 = 12$, $T_1 = \frac{0.1}{4W}$, and $T_2 = \frac{NT}{N_2}$, there is 34 dB cancellation for the first level and 55 dB for the overall two-level cancellation. Interestingly, the two-level uniform canceler does not provide improvement over the single-level uniform canceler.

Chapter 8

Conclusion

8.1 Summary of Contributions

The contributions in the area of optimal industrial load control in smart grid are as follows:

- Industrial load control optimization problem under two cases are formulated: basic and comprehensive. In the basic case, amount of material processed by a unit is not included in the formulation and the only decision variables of the optimization problem are the status (on/off) of the operation of the units at each time slot. This case can be applicable to the industries where each industrial unit is processing a constant amount of material at each cycle and its electricity load is constant at each cycle. In the comprehensive case, amount of material processed by a unit is included as a decision variable. This case can be applicable to the industries where an industrial unit may take different amount of material at each cycle and its electricity load has

an affine relationship with the amount of material processed.

- Several industrial load constraints are considered in the formulation including inter-dependency among industrial units, uninterruptiblity of the industrial units, materials that should be consumed as as soon as they are produced, and maximum load constraint. In the comprehensive case material-related constraints such as material balance, material proportionality, and material storage are also considered.

- Operation under different smart pricing scenarios are considered: day-ahead pricing, time-of-use pricing, peak pricing, inclining block rates, and critical peak pricing. The use of behind-the-meter renewable generation and energy storage are also taken into consideration.

- The formulated industrial load control optimization problem is a tractable linear mixed-integer program.

- Case studies include illustrative examples. Also, scenarios based on an oil refinery and a steel mill industry are presented.

The contributions in the area of full-duplex are as follows:

- A novel architecture for an all-analog canceler, clustered canceler, is proposed.

- Through simulation, it is shown that in addition that the performance of the clustered canceler is as good or better than the uniform canceler, its performance is also independent of the carrier frequency.

- A statistical evaluation of the performance of both all-analog cancelers, clustered and uniform cancelers, for ideal and non-ideal attenuators is provided. These results can be used for guiding expectations of results and the implementation of more ambitious and thorough hardware-based experiments.

8.2 Future Work

The future work in the area of optimal industrial load control in smart grid are as follows:

- To extend the proposed ILC formulation to include industrial units that consume different amount of energy during a cycle.
- Also to extend the proposed formulation to include other type of energies rather than electricity only. For example, a *combined* electricity and natural gas optimization can be considered. In addition, *on-site* electricity production, where the industrial complex produces its own electricity on-site rather than purchasing from the utility, would also be considered.
- To study the impact of optimal industrial load control on carbon foot-print *emission* of an industrial complex.
- To use the proposed formulation to uncover the *bottlenecks* of an industrial complex as shortly explained in Section 5.3.1.

The future work in the area of full-duplex is as follows:

- To implement the all-analog architecture on hardware and compare results from hardware with the simulation results.

Appendix A

Steel Industry

There are two process routes that dominate steel manufacturing: integrated and mini-mill routes. The key difference between the two is the type of iron bearing feedstock they consume. In an integrated works this is mainly iron ore, with a smaller quantity of steel scrap, while in a mini-mill this is mainly steel scrap, or increasingly, other sources of metallic iron such as directly reduced iron.

In integrated route, first iron must be made and then iron is converted to steel. Raw materials for the process include iron ore, coal, limestone, steel scrap (Scrap use is also an essential aspect of steelmaking BOF process that requires about 10% to 30% of scrap as a feed material to operate correctly), and a wide range of other materials in variable quantities such as oil, air, chemicals, refractories, alloys, and water. Iron from the blast furnace is converted to steel in the Basic Oxygen Furnace (BOF) and after casting and solidification, is formed into coil, plate, sections or bars in dedicated rolling mills. The integrated steelmaking route accounts for about 60% of world steel production [41]. The

flow diagram of an integrated route is shown in Fig. A.1.

In mini-mill route, steel is made in an electric arc furnace (EAF) by melting recycled scrap in an EAF and adjusting the chemical composition of the metal by adding alloying elements, usually in a lower powered ladle furnace (LF). Note that in mini-mill route, the ironmaking processes, operated on the integrated plant, are not required. Most of the energy for melting comes from electricity. In addition to steel scrap, metallic substitutes such as direct reduced iron (DRI) are becoming more important since scrap availability is limited. Over 40% of world steel is manufactured using processes that consume scrap as the primary input material [41]. The flow diagram of a mini-mill route is shown in Fig. 4.1.

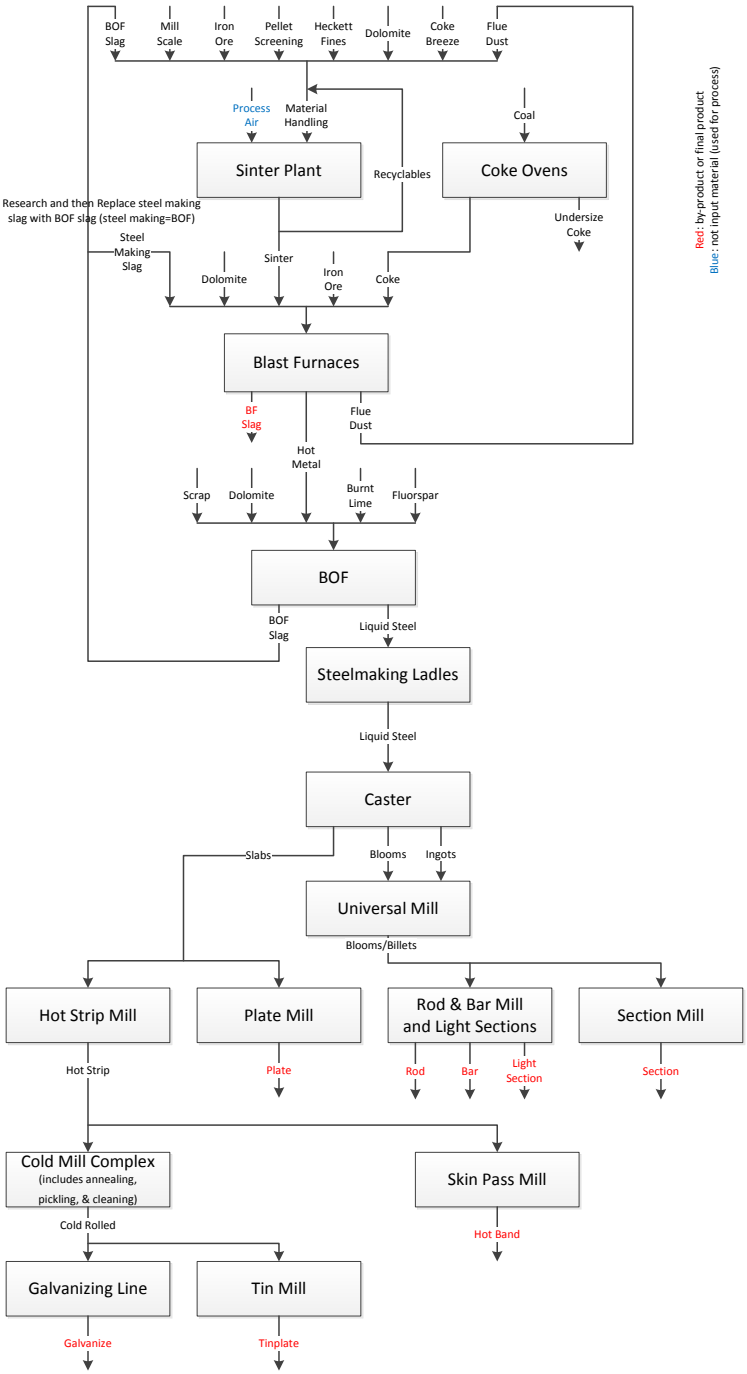

Figure A.1: Flow diagram of an integrated route.

Glossary

CPP Critical Peak Pricing. 46

CPU Catalytic Polymerisation Unit. 21

DAP Day-Ahead. 44

DLC direct load control. 2

DR demand response. 13

DRI direct reduced iron. 106

EAF electric arc furnace. 106

IBR Inclining Block Rates. 45

ILC Industrial Load Control. 13

LF ladle furnace. 106

LP linear programming. 7

LPG liquid petroleum gas. 20

MILP mixed-integer linear program. 9

MIP mixed-integer program. 9

PAR peak-to-average ratio. 13

PP Peak Pricing. 44

PPU1 Propane Production Unit 1. 21

QP quadratic programming. 9

SIC self-interference cancellation. 76

ToUP Time-of-Use Pricing. 44

Bibliography

[1] A. Gholian, H. Mohsenian-Rad, Y. Hua, and J. Qin, "Optimal industrial load control in smart grid: A case study for oil refineries," in *Power and Energy Society General Meeting, 2013 IEEE.* IEEE, 2013.

[2] A. Gholian, H. Mohsenian-Rad, and Y. Hua, "Optimal industrial load control in smart grid," *submitted to IEEE Trans. on Smart Grid*, 2014.

[3] A. Gholian, Y. Ma, and Y. Hua, "A numerical investigation of all-analog radio self-interference cancellation," in *Signal Processing Advances in Wireless Communications (SPAWC), 2014 IEEE 15th International Workshop on.* IEEE, 2014, pp. 459–463.

[4] Y. Hua, Y. Ma, A. Gholian, Y. Li, A. C. Cirik, and P. Liang, "Radio self-interference cancellation by transmit beamforming, all-analog cancellation and blind digital tuning," *Signal Processing*, vol. 108, pp. 322–340, 2015.

[5] D. G. Luenberger, *Introduction to linear and nonlinear programming.* Addison-Wesley Reading, MA, 1973, vol. 28.

[6] E. K. Chong and S. H. Zak, *An introduction to optimization.* John Wiley & Sons, 2013, vol. 76.

[7] S. Boyd and L. Vandenberghe, *Convex optimization.* Cambridge university press, 2009.

[8] M. Grant, S. Boyd, and Y. Ye, "Cvx: Matlab software for disciplined convex programming," 2008.

[9] C. A. Floudas, *Nonlinear and mixed-integer optimization: fundamentals and applications.* Oxford University Press, 1995.

[10] "Ibm ilog cplex 12.5 users manual," http://www-01.ibm.com/software/commerce/optimization/cplex-optimizer.

[11] "Mosek optimization software," http://www.mosek.com.

[12] C. Joe-Wong, S. Sen, S. Ha, and M. Chiang, "Optimized day-ahead pricing for smart grids with device-specific scheduling flexibility," *Selected Areas in Communications, IEEE Journal on*, vol. 30, no. 6, pp. 1075–1085, 2012.

[13] J.-N. Sheen, C.-S. Chen, and T.-Y. Wang, "Response of large industrial customers to electricity pricing by voluntary time-of-use in taiwan," in *Generation, Transmission and Distribution, IEEE Proceedings*, vol. 142, no. 2. IET, 1995, pp. 157–166.

[14] P. H. Jayantilal and N. Shah, "A review on electrical energy management techniques for supply and consumer side in industries," *Int. Journal of Scientific Engineering and Technology Research*, vol. 3, pp. 550–556, Apr. 2014.

[15] A. V. Stokke, G. L. Doorman, and T. Ericson, "An analysis of a demand charge electricity grid tariff in the residential sector," *Energy Efficiency*, vol. 3, no. 3, pp. 267–282, 2010.

[16] P. Samadi, H. Mohsenian-Rad, V. W. Wong, and R. Schober, "Tackling the load uncertainty challenges for energy consumption scheduling in smart grid," *Smart Grid, IEEE Transactions on*, vol. 4, no. 2, pp. 1007–1016, 2013.

[17] A. Bego, L. Li, and Z. Sun, "Identification of reservation capacity in critical peak pricing electricity demand response program for sustainable manufacturing systems," *International Journal of Energy Research*, vol. 38, no. 6, pp. 728–736, 2014.

[18] A.-H. Mohsenian-Rad and A. Leon-Garcia, "Optimal residential load control with price prediction in real-time electricity pricing environments," *IEEE Trans. on Smart Grid*, vol. 1, no. 2, pp. 120–133, 2010.

[19] Y. Guo, M. Pan, and Y. Fang, "Optimal power management of residential customers in the smart grid," *IEEE Trans. on Parallel and Distributed Systems*, vol. 23, no. 9, pp. 1593–1606, 2012.

[20] N. Gatsis and G. B. Giannakis, "Residential load control: Distributed scheduling and convergence with lost ami messages," *Smart Grid, IEEE Transactions on*, vol. 3, no. 2, pp. 770–786, 2012.

[21] S. Datchanamoorthy, S. Kumar, Y. Ozturk, and G. Lee, "Optimal time-of-use pricing for residential load control," in *Smart Grid Communications (SmartGridComm), 2011 IEEE International Conference on*. IEEE, 2011, pp. 375–380.

[22] M. A. P. S. Kiliccote and D. Hansen, "Advanced controls and communications for demand response and energy efficiency in commercial buildings," *Proceedings of Second Carnegie Mellon Conference in Electric Power Systems*, Jan. 2006.

[23] H. Hao, A. Kowli, Y. Lin, P. Barooah, and S. Meyn, "Ancillary service for the grid via control of commercial building hvac systems," in *American Control Conference (ACC), 2013*. IEEE, 2013, pp. 467–472.

[24] C. A. Floudas and X. Lin, "Continuous-time versus discrete-time approaches for scheduling of chemical processes: a review," *Computers & Chemical Engineering*, vol. 28, no. 11, pp. 2109–2129, 2004.

[25] Y. Ding and S. H. Hong, "A model of demand response energy management system in industrial facilities," in *Proc. of IEEE SmartGridComm*, Vancouver, Canada, Nov. 2013.

[26] S. Bahrami, F. Khazaeli, and M. Parniani, "Industrial load scheduling in smart power grids," in *22nd International Conference on Electricity Distribution*, 2013.

[27] S. Ashok and R. Banerjee, "An optimization mode for industrial load management," *IEEE Trans. on Power Systems*, vol. 16, no. 4, pp. 879–884, 2001.

[28] S. Ashok, "Peak-load management in steel plants," *Applied Energy*, vol. 83, no. 5, pp. 413–424, 2006.

[29] C. Babu and S. Ashok, "Peak load management in electrolytic process industries," *IEEE Trans. on Power Systems*, vol. 23, no. 2, pp. 399–405, 2008.

[30] B. Zhang and B. Hua, "Effective milp model for oil refinery-wide production planning and better energy utilization," *Journal of Cleaner Production*, vol. 15, no. 5, pp. 439–448, 2007.

[31] "BP kwinana refinery- public environmental report," Tech. Rep., Jan. 2011. [Online]. Available: http://tinyurl.com/PER-BP-Kwinana-2009

[32] E. Worrell and C. Galitsky, "An ENERGY STAR guide for energy and plant managers," Tech. Rep., 2005.

[33] A.-H. Mohsenian-Rad and A. Leon-Garcia, "Optimal residential load control with price prediction in real-time electricity pricing environments," *Smart Grid, IEEE Transactions on*, vol. 1, no. 2, pp. 120–133, 2010.

[34] [Online]. Available: https://www2.ameren.com/RetailEnergy/RtpDownload

[35] [Online]. Available: http://www.pge.com/en/mybusiness/rates/tvp/toupricing.page

[36] [Online]. Available: http://www.riversideca.gov/utilities/pdf/2013/Electric%20Schedule%20TOU-%20clean%202-1-2013.pdf

[37] [Online]. Available: http://www.fcgov.com/utilities/business/rates/electric/coincident-peak

[38] Z. Liu, A. Wierman, Y. Chen, B. Razon, and N. Chen, "Data center demand response: Avoiding the coincident peak via workload shifting and local generation," *Performance Evaluation*, vol. 70, no. 10, pp. 770–791, 2013.

[39] [Online]. Available: http://www.worldsteel.org/dms/internetDocumentList/fact-sheets/fact_energy_2014/document/fact_energy_2014.pdf

[40] [Online]. Available: http://calculatelca.com/wp-content/themes/athena/images/LCA%20Reports/Steel_Production.pdf

[41] I. Iron and U. N. E. P. D. of Technology, *Industry as a Partner for Sustainable Development: Iron and Steel*. UNEP/Earthprint, 2002, vol. 21.

[42] [Online]. Available: http://www.steelonthenet.com/cost-eaf.html

[43] [Online]. Available: http://www.phoenixsteelservice.com

[44] [Online]. Available: http://www.steelonthenet.com/steel-prices.html

[45] http://www.pjm.com/markets-and-operations/energy/real-time/monthlylmp.aspx.

[46] http://www-metdat.llnl.gov/cgi-pub/reports/simple_report.pl.

[47] Y. Hua, Y. Ma, P. Liang, and A. Cirik, "Breaking the barrier of transmission noise in full-duplex radio," in *MILCOM 2013*.

[48] J. I. Choi, M. Jain, K. Srinivasan, P. Levis, and S. Katti, "Achieving single channel, full duplex wireless communication," in *Proceedings of the sixteenth annual international conference on Mobile computing and networking*. ACM, 2010, pp. 1–12.

[49] S. S. Hong, J. Mehlman, and S. Katti, "Picasso: flexible rf and spectrum slicing," *ACM SIGCOMM Computer Communication Review*, vol. 42, no. 4, pp. 37–48, 2012.

[50] J. G. McMichael and K. E. Kolodziej, "Optimal tuning of analog self-interference cancellers for full-duplex wireless communication," in *Communication, Control, and Computing (Allerton), 2012 50th Annual Allerton Conference on*. IEEE, 2012, pp. 246–251.

[51] D. Bharadia, E. McMilin, and S. Katti, "Full duplex radios," in *Proceedings of the ACM SIGCOMM 2013 conference on SIGCOMM*. ACM, 2013, pp. 375–386.

[52] Y. Choi and H. Shirani-Mehr, "Simultaneous transmission and reception: Algorithm, design and system level performance," *IEEE Transactions on Wireless Communications, to appear*.

[53] M. A. Khojastepour and S. Rangarajan, "Wideband digital cancellation for full-duplex communications," in *Signals, Systems and Computers (ASILOMAR), 2012 Conference Record of the Forty Sixth Asilomar Conference on*. IEEE, 2012, pp. 1300–1304.

[54] M. Duarte and A. Sabharwal, "Full-duplex wireless communications using off-the-shelf radios: Feasibility and first results," in *Signals, Systems and Computers (ASILOMAR), 2010 Conference Record of the Forty Fourth Asilomar Conference on*. IEEE, 2010, pp. 1558–1562.

[55] A. Sahai, G. Patel, and A. Sabharwal, "Pushing the limits of full-duplex: Design and real-time implementation," 2011.

[56] Y. Hua, P. Liang, Y. Ma, A. C. Cirik, and Q. Gao, "A method for broadband full-duplex mimo radio," *Signal Processing Letters, IEEE*, vol. 19, no. 12, pp. 793–796, 2012.

[57] M. Jain, J. I. Choi, T. Kim, D. Bharadia, S. Seth, K. Srinivasan, P. Levis, S. Katti, and P. Sinha, "Practical, real-time, full duplex wireless," in *Proceedings of the 17th annual international conference on Mobile computing and networking*. ACM, 2011, pp. 301–312.